Theoretical study of narrow band high frequency clicks from small dolphins : models and measures

Franck Malige, Julie Patris, Gisela Giardino, Diego Horacio Rodriguez, Hervé Glotin

Research report

Franck MALIGE[(a)], Julie PATRIS[(b)], Gisela GIARDINO[(c)], Diego Horacio RODRIGUEZ[(c)], Hervé GLOTIN [(a)]

(a) DYNI Team, LIS, université de Toulon
(b) Université d'Aix-Marseille
(c) IIMyC, Universidad Nacional Mar del Plata

November 2022

Theoretical study of narrow band high frequency clicks from small dolphins : models and measures

Contents

Introduction

In this report, we seek to evaluate the interest of a method for estimating the click parameters of NBHF (Narrow band high frequency) clicks of dolphins based on Gabor wavelet mathematical models. For this, we compare this method with more traditional ways of estimating these parameters. The aim of this study is to find a method that would allow to effectively separate species of coastal dolphins that have similar vocal behavior. In particular, when we have a medium or long term follow-up, without visual counterpart and when many clicks are detected.

1 Preliminary description of clicks, parameters and difficulties

1.1 Description of coastal dolphin clicks from Chile, general issue

The clicks and buzz recorded in the Puyuhuapi channel in May 2021 (Patris et al. 2023) are very likely Chilean dolphin clicks (*Cephalorhynchus eutropia*). These are very brief sound emissions, of the order of a few tens of μs and very high frequency, the energy usually being above 100 kHz. However, this could also be clicks from Peale's dolphins (*Lagenorhynchus australis*) or Burmeister's porpoise (*Phocoena spinipinnis*). The clicks recorded in December 2021 in the Strait of Magellan are clicks of Peale's dolphins (*Lagenorhynchus australis*) and those recorded at Llico in October 2022 are of dolphins Chileans (*Cephalorhynchus eutropia*) (visual confirmation in both cases). These species do not seem to emit whistles but sometimes emit buzzes, when the clicks are emitted in large numbers in a short time (the time between two clicks can go down around 2 ms). In figure 1, we recall the waveform and spectrum of the clicks of these three species described in former papers. These three species have very similar vocal behavior and a current challenge is to be able to separate them on the basis of their sound emissions alone.

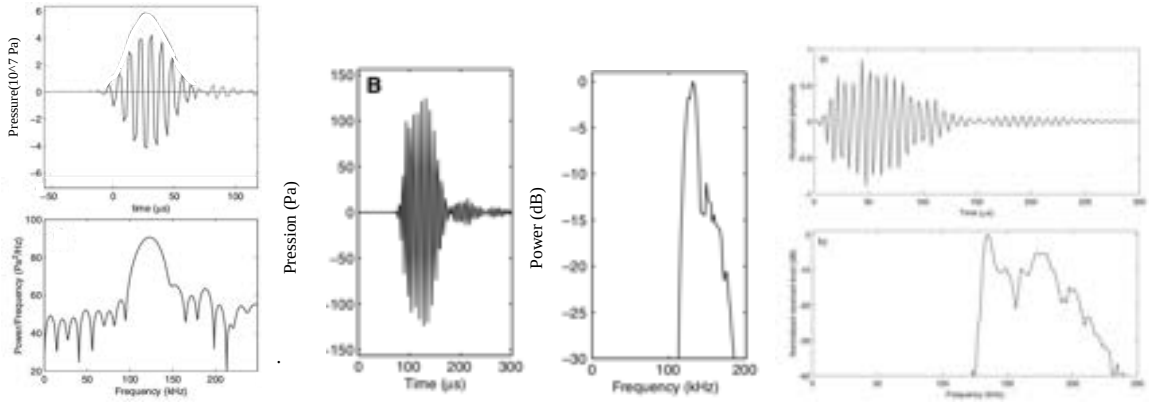

Figure 1: Left : typical click of a Chilean dolphin (*Cephalorhynchus eutropia*), waveform and spectrum (Götz et al. 2010). In the center : typical click of a Peale's dolphin (*Lagenorhynchus australis*), waveform and spectrum (Kyhn et al. 2010). Right: typical click of a Burmeister's Porpoise (*Phocoena spinipinnis*) waveform and spectrum (Reyes Reyes et al. 2018). All these recordings had a sampling frequency of 500kHz.

1.2 Click parameters typically used in bioacoustic studies and issues with using them

To acoustically describe the type of clicks emitted by small cetaceans, many classic indicators are used in bioacoustics. Since Au (1993), there has been a **relative standardization of the measurements** carried out on dolphin clicks. This standardization allows reproducibility of the measurements and the declared aim is often to find a way to differentiate species with similar vocal behaviors (Reyes Reyes et al. 2018). This type of method makes it possible, for example, to effectively separate bottlenose dolphins (*Tursiops truncatus*) and NBHF dolphins, the former having a much lower peak frequency and a much wider bandwidth than the seconds (Kamminga et al. 1996).

The majority of the characteristics of these signals are divided into two dual categories, a temporal category and a frequency category. Among the temporal characteristics, we can note : the average date of the signal, the duration characteristic at -10dB ($\Delta_{t\ (10dB)}$) and at -20dB ($\Delta_{t\ (20dB)}$), the characteristic duration 'rms' (for 'root mean square'). Among the frequency characteristics, we can note : the 'peak' frequency f_p of the signal, the 'centroid' frequency f_c, the bandwidths at -10dB y -3dB ($\Delta_{f\ (-10dB)}$ and $\Delta_{f\ (-3dB)}$), the characteristic bandwidth 'rms' and the factor of

quality at -3dB ($Q_{\ (3dB)}$). The definitions of the parameters associated with a signal $s(t)$ (and its Fourier transform, defined by the formula $S(f) = \int_{-\infty}^{+\infty} s(t)e^{-2i\pi ft}dt$) are (Au 1993) :

- The energy of the signal $E = \int_{-\infty}^{+\infty} |s(t)|^2 dt \ = \int_{-\infty}^{+\infty} |S(f)|^2 df$
- The amplitude of the signal, which is the maximum value of the signal s
- The amplitude peak-to-peak of the signal, which is the maximum value minus the minimum value of s
- The mean date of the signal defined by $t_c = \frac{\int_{-\infty}^{+\infty} t|s(t)|^2 dt}{\int_{-\infty}^{+\infty} |s(t)|^2 dt}$.
- The duration 'rms' : $\Delta t = \sqrt{\frac{\int_{-\infty}^{+\infty} (t-t_c)^2|s(t)|^2 dt}{\int_{-\infty}^{+\infty} |s(t)|^2 dt}}$.
- The duration at -10dB ($\Delta t_{\ (-10dB)}$) is defined as the duration when the envelope of the signal is above the maximum of the envelope divided by $\sqrt{10}$. In practice, we get the envelope taking the modulus of the Hilbert transform of the signal.
- The duration at -20dB ($\Delta t_{\ (-20dB)}$) is defined as the duration when the envelope of the signal is above the maximum of the envelope divided by 10
- The peak frequency f_p du signal is the frequency where the spectrum $|S(f)|$ of the signal is maximum.
- The 'centroïde' frequency f_c is defined by the formula $f_c = \frac{\int_{-\infty}^{+\infty} f|S(f)|^2 df}{\int_{-\infty}^{+\infty} |S(f)|^2 df}$.
- The 'rms' bandwidth : $\Delta f = \sqrt{\frac{\int_{-\infty}^{+\infty} (f-f_c)^2|S(f)|^2 df}{\int_{-\infty}^{+\infty} |S(f)|^2 df}}$
- The bandwidth at -3dB ($\Delta f_{\ (-3dB)}$) is the length of the interval around f_p where the modulus of the spectrum is larger than $\frac{max(|S(f)|)}{\sqrt{2}}$ (it is equivalent to $max(|S(f)|^2 - 3$dB when $max(|S(f)|^2$ is in $dB)$.
- The bandwidth at -10dB ($\Delta f_{\ (-10dB)}$) is the length of the interval around f_p where the modulus of the spectrum is larger $\frac{max(|S(f)|^2)}{\sqrt{10}}$.
- The quality factor at -3dB is $Q_{\ (3dB)} = \frac{f_c}{\Delta f_{(-3dB)}}$.
- The quality factor 'rms' is $Q_{rms} = \frac{f_c}{\Delta f}$.
- The duration-bandwidth product 'rms' is $\Delta t \times \Delta f = \sqrt{\frac{\int_{-\infty}^{+\infty} (t-t_c)^2|s(t)|^2 dt}{\int_{-\infty}^{+\infty} |s(t)|^2 dt}} \times \sqrt{\frac{\int_{-\infty}^{+\infty} (f-f_c)^2|S(f)|^2 df}{\int_{-\infty}^{+\infty} |S(f)|^2 df}}$

Remark : it should be noted that the functions $|s(t)|^2 / \int_{-\infty}^{+\infty} |s(t)|^2 dt$ and $|S(f)|^2 / \int_{-\infty}^{+\infty} |S(f)|^2 df$ are considered as probability densities of the random variables t and f. When we compute t_c and f_c, we compute the first order moments of these random variables. When we compute Δt and Δf, we compute the second order centered moments of these random variables.

For the three species of Chilean coastal dolphins mentioned above, articles and reports have measured all or part of these parameters (Rojas-Mena 2009; Götz et al. 2010; Kyhn et al. 2010; Reyes Reyes et al. 2018; Patris et al. 2023). The majority of these indicators describe the frequency content of the signal and are generally used to classify, by statistical methods, the different species (Rojas-Mena 2009; Reyes Reyes et al. 2018). Nevertheless, it is important to note several flaws in the calculation of these parameters :

- The indicators used are not always the same from one article to another and there is no consensus, among bioacousticians studying dolphins, on which are the most interesting to classify clicks.
- Some of these parameters are not well defined. As an example, the centroid frequency (whose definition given above corresponds to the average of the frequency considering the energy in the spectrum) is defined as such in Rojas-Mena (2009); Götz et al. (2010); Reyes Reyes et al. (2018). But it is sometimes defined as the median of the energy distribution in the spectrum (Kyhn et al. 2010; Reyes Reyes et al. 2015). And in some studies, the two values of the centroid frequency are compared (Reyes Reyes et al. 2018). This confusion is already present in Au (1993), p 217.

- These parameters are often closely linked or even redundant, in particular the different frequency measurements (peak or centroid), duration or bandwidth, which complicates the work of classification.
- Even if the cited studies present statistical indicators of data dispersion, there is rarely a study of the error made in estimating these parameters. Dispersion that may come from the diversity of emissions but also from the measure of the signals.
- Signals recorded in the field often have one or more replicas and these replicas have a significant influence on the calculation of the parameters and therefore their accuracy (see section 3).

Finally, the parameters calculated for the three species mentioned above are often quite similar (Rojas-Mena 2009; Reyes Reyes et al. 2018), which implies the need to find indicators with few errors of measure to be able (perhaps) to discriminate between them. For all these reasons, classification is not easy even after calculation of these indicators and no reliable classification method resulting from the measurement of these parameters has been offered until now. In an attempt to improve the classification and clarify the importance of these parameters, we propose the study of another method, already used for other species, which is the adjustment of a mathematic function to these signals.

2 Gabor wavelet

2.1 Definition

The clicks of dolphins presented in figure 1 are signals which seem to be able to be approximated by a simple math model : Gabor wavelets.

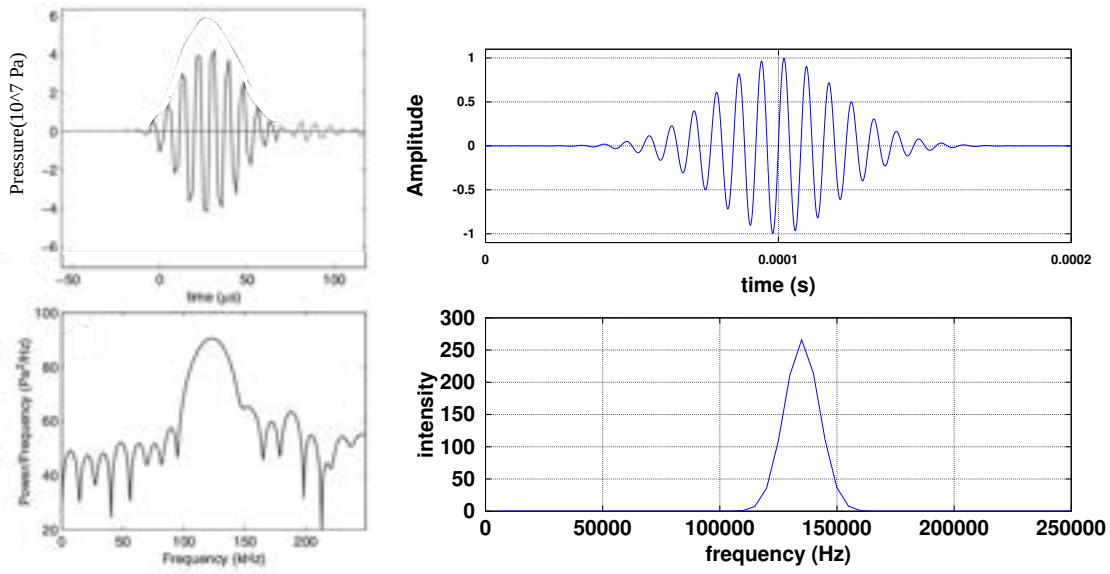

Figure 2: Left : waveform (above) et spectrogram (below) of a typical clic form a Chilean dolfin (*Cephalorhynchus eutropia*) (Götz et al. 2010) - sampling frequency of 500 kHz. Right : a Gabor wavelet, with $f_0 = 130kHz$, $T = 200\mu s$ and $\phi = 0$ and a sampling frequency of $10GHz$

These signals, in waveform, centered on the date t_0 are given by the formula:

$$g(t) = A\ e^{-\frac{(t-t_0)^2}{T^2}}\ cos(2\pi f_0(t-t_0)+\phi) \tag{1}$$

These are mathematical functions obtained by the multiplication of an amplitude A, of a Gaussian, centered at t_0 and standard deviation $\sigma = \frac{T}{2}$ and a cosine function of frequency f_0 and phase shift ϕ at $t = t_0$. These wavelets are therefore defined by 5 parameters (t_0, A, T, f_0 and ϕ): t_0 is the central time of the wavelet, A is the amplitude, f_0 the frequency of the fast oscillations of the wavelet given by the cosine, T the characteristic time of duration of the wavelet and ϕ the phase difference between the Gaussian and the cosine. These wavelets are very similar to dolphins NBHF clicks presented in figure 1 and in figure 2. The Gaussian $A\ e^{-\frac{(t-t_0)^2}{T^2}}$ is the envelope of the signal. Note that

the parameters which seem the most important to properly characterize the Gabor wavelets are the time T and the frequency f_0. One of the most important traits of coastal dolphin clicks is that they are narrow bandwidth, which is related to the fact that we "see" a lot of cosine oscillations before the Gaussian becomes very weak : we are in the case where $\frac{1}{T} << f_0$ or, equivalently $T_0 << T$ where $T_0 = \frac{1}{T_0}$ corresponds to the period of the cosine. These signals have been named **polycyclic** (we see several oscillations) in opposition to **oligocyclic** signals, such as clicks of Tursiops, for example, which usually have less than four visible oscillations (Kamminga et al. 1996) or sperm whale clicks (Goold and Jones 1995).

This representation of the clicks of small dolphins through a Gabor wavelet was proposed there already several decades in a series of articles, by C. Kamminga and other authors, entitled "Investigation on cetacean sonars" (articles I to XI published in Aquatic mammals in the 80s): for example for the family phocoenidae (Kamminga et al. 1996) or to compare species (Wiersma 1982). More recently, an article models the click production of *Tursiops truncatus* and *Phocoena phocoena* by Gabor wavelets (Wei et al. 2020). It can also be noted that other mathematical models modeling the waveform of dolphin clicks have been proposed, more sporadically, essentially to model their production (Dubrovsky et al. 2004). The signals recorded in the field are not exactly Gabor wavelets but Gabor wavelets can be considered as a first good approximation of these signals. We can try to adjust a wavelet to the real signal and measure the difference with a real signal. These wavelets can be considered as a standard signal against which we will measure our signals.

2.2 Classical parameters for Gabor wavelets

In this section, we calculate precisely the classical parameters presented in section 1.2 for a Gabor wavelet, in the case of narrow frequency band signals (i.e. in the case where $T_0 << T$).

2.2.1 Analitic signal associated to a Gabor wavelet

.

Another Gabor wavelet model is the complex Gabor wavelet :

$$\mathrm{g}(t) = Ae^{-\frac{(t-t_0)^2}{T^2}}\ e^{2i\pi f_0(t-t_0)+i\phi} \tag{2}$$

The advantage of this wavelet is the greater simplicity of the calculations of the parameters mentioned above. For example, the Fourier transform of g is

$$\underline{\mathrm{G}}(f) = \sqrt{\pi}ATe^{-\pi^2T^2(f-f_0)^2}e^{-2i\pi ft_0+i\phi} \tag{3}$$

The proof is given in appendix 6. It is interesting to note that the Fourier transform of the signal complex is also a complex Gabor wavelet centered at f_0 and that its standard deviation is proportional to $\frac{1}{T}$. It is the same remark than formulated in the previous section : the larger T is, the more the Fourier transform will be stitched around f_0 (and hence narrower the bandwidth). This expression makes it easy to calculate the Fourier transform of g (demonstration given in appendix 6), which is

$$G(f) = \frac{\sqrt{\pi}AT}{2}[e^{-\pi^2T^2(f-f_0)^2}e^{-2i\pi ft_0+i\phi} + e^{-\pi^2T^2(f+f_0)^2}e^{-2i\pi ft_0-i\phi}] \tag{4}$$

An analytical signal $y(t)$ is a signal for which the spectrum $Y(f)$ is equal to zero for negative frequencies (Ville 1948; Rihaczek 1996). We can associate to any signal $y(t)$ an associated analytical signal which is defined by $y_a(t) = y(t) + i\sigma(t)$ where $\sigma(t)$ is the Hilbert transform of y. In view of the expression of the Fourier transform of the Gabor wavelet real (equation 4), the spectrum is not zero for negative frequencies, especially when f is close to $-f_0$ and is roughly the sum of two Gaussian peaks, one centered at f_0 and te other at $-f_0$. Nevertheless, in the case where $\pi^2T^2f_0^2$ is large compared to 1 (case of polycyclic clicks), we can consider that these two peaks are well separated and that, for example, $e^{-\pi^2T^2(f+f_0)^2} \simeq 0$ when f is positive. This is the case of coastal dolphins recorded in the Puyuhuapi channel and more generally in the studies available on the three coastal dolphin species (Rojas-Mena 2009; Götz et al. 2010; Kyhn et al. 2010; Reyes Reyes et al. 2018). Indeed, f_0 is of the order of 100 kHz and T more than 10 μs for these signals, which gives $\pi^2T^2f_0^2 \gtrsim 10$ and therefore $e^{-\pi^2T^2f_0^2} < 5.10^{-5}$. In this case, one can consider that the analytical signal associated with the real Gabor wavelet is the complex Gabor wavelet (Rihaczek 1996).

Table 1: List of computed parameters for Gabor Wavelets

signal	symbol	Complex Gabor wavelet	Real Gabor wavelet
Signal	$s(t)$	$\underline{g}(t) = Ae^{-\frac{(t-t_0)^2}{T^2}} e^{2i\pi f_0(t-t_0)+i\phi}$	$g(t) = Ae^{-\frac{(t-t_0)^2}{T^2}} cos(2\pi f_0(t-t_0)+\phi)$
Fourier transform	$S(f)$	$\underline{G}(t) = \sqrt{\pi}ATe^{-\pi^2T^2(f-f_0)^2}e^{-2i\pi ft_0+i\phi}$	$G(t) = \frac{\sqrt{\pi}AT}{2}e^{-2i\pi ft_0}[e^{-\pi^2T^2(f-f_0)^2}e^{i\phi} + e^{-\pi^2T^2(f+f_0)^2}e^{-i\phi}]$
Energy	E	$\sqrt{\frac{\pi}{2}}A^2T$	$\sqrt{\frac{\pi}{2}}A^2T\ [1+cos(2\phi)e^{-2\pi^2{f_0}^2T^2}] \simeq \sqrt{\frac{\pi}{2}}A^2T$
Average date	t_c	t_0	$t_0 - \pi f_0T^2\frac{sin(2\phi)}{cos(2\phi)+e^{2\pi^2{f_0}^2T^2}} \simeq t_0$
Duration at -10dB	Δt_{-10dB}	$\sqrt{2ln(10)}\ T \simeq 2.15\ T$	$\sqrt{2ln(10)}\ T \simeq 2.15\ T$
Duration at -20dB	Δt_{-20dB}	$\sqrt{4ln(10)}\ T \simeq 3.03\ T$	$\sqrt{4ln(10)}\ T \simeq 3.03\ T$
Duration 'rms'	Δt	$\frac{1}{2}\ T$	$\frac{1}{2}\ T\ \frac{1+cos(2\phi)e^{-2\pi^2{f_0}^2T^2(1-8\pi{f_0}^2T^2)}}{1+cos(2\phi)e^{-2\pi^2{f_0}^2T^2}} \simeq \frac{1}{2}\ T$
Peak frequency	f_p	f_0	$\simeq f_0$ ou $-f_0$
Centroïd frequency	f_c	f_0	0
Bandwidth at -3dB	Δf_{-3dB}	$\frac{\sqrt{2ln(2)}}{\pi}\ \frac{1}{T} \simeq 0.37\ \frac{1}{T}$	$\simeq \frac{\sqrt{2ln(2)}}{\pi}\ \frac{1}{T} \simeq 0.37\ \frac{1}{T}$
Bandwidth at -10dB	Δf_{-10dB}	$\frac{\sqrt{2ln(10)}}{\pi}\ \frac{1}{T} \simeq 0.68\ \frac{1}{T}$	$\simeq \frac{\sqrt{2ln(10)}}{\pi}\ \frac{1}{T} \simeq 0.68\ \frac{1}{T}$
Bandwidth 'rms'	Δf	$\frac{1}{2\pi}\ \frac{1}{T} \simeq 0.16\ \frac{1}{T}$	$\simeq \frac{1}{2\pi}\ \frac{1}{T} \simeq 0.16\ \frac{1}{T}$
Quality factor at -3dB	Q_{-3dB}	$\frac{\pi}{\sqrt{2ln(2)}}\ f_0T \simeq 2.67\ f_0T$	$\simeq \frac{\pi}{\sqrt{2ln(2)}}\ f_0T \simeq 2.67\ f_0T$
Quality factor 'rms'	Q_{rms}	$2\pi f_0T \simeq 6.28\ f_0T$	$\simeq 2\pi f_0T \simeq 6.28\ f_0T$
'rms' duration-bandwidth product or uncertainty product	P_{incert}	$\frac{1}{4\pi}$	$\simeq \frac{1}{4\pi}$
Autocorrelation function	$C(r)$	$\sqrt{\frac{\pi}{2}}A^2T\ e^{-\frac{r^2}{2T^2}}\ e^{-2i\pi f_0r}$	$\simeq \frac{1}{2}\sqrt{\frac{\pi}{2}}A^2T\ e^{-\frac{r^2}{2T^2}}\ cos(2\pi f_0r)$

2.2.2 Computation of parameters for Gabor wavelets and remarks

The parameters of complex and real Gabor wavelets are presented in table 1 and their calculation is detailed in appendix 6. A series of remarks can be made on the calculations presented in this table.

- If we consider that the clicks studied are "polycyclic" (i.e. $\pi^2{f_0}^2T^2 >> 1$), which is the case for dolphins coastal, then the parameters for complex and real Gabor wavelets are very close. This is due to the fact, noted above, that in this case the analytical signal associated with the real Gabor wavelet is very close to the complex Gabor wavelet.

- The frequencies f_p and f_c are close to f_0 and therefore are good indicators of this value. We can also notice that the centroid frequency of the real signal is zero, by symmetry of the spectrum.

- The durations presented in table 1 are all proportional to the single parameter T, which means that they are very redundant to measure the signal or to classify the clicks if we assume that the clicks are close to Gabor wavelets. In the same way, the bandwidths presented in table 1 are all proportional to the single parameter $\frac{1}{T}$, which means that they are very redundant for measuring the signal. They are therefore also redundant with the durations presented. A statistical correlation table between the parameters is presented in (Rojas-Mena 2009) : in this table, we find the correlations or anti-correlations highlighted above, between f_p and f_c but also between all bandwidths and durations. Overall, if we are in presence of a signal close to a Gabor wavelet, this table shows that a lot of these parameters are highly correlated and that it is surely wise to keep only a few of them for classification.

- The two quality factors presented are proportional to the product $f_0T = \frac{T}{T_0}$ and are therefore also proportional the number of oscillations that we see in the signal: the greater the quality factor, the more we are in the case of a polycyclic signal.

- The uncertainty product of a Gabor wavelet is $\frac{1}{4\pi}$. One can prove (Gabor 1946), that uncertainty product is always greater than $\frac{1}{4\pi}$ for any signal, the minimum being precisely reached for the Gabor wavelets. Several articles thus measure how the real signals approach this limit for different species (Kamminga et al. 1986, 1993).

From all these remarks and from the fact that the measured clicks are close to Gabor wavelets, it is indicated, for the purpose of precise characterization of the signal and classification, to retain only a few parameters among those of table 1. In the following sections, we will present the theoretical estimate and practical frequency, duration and signal bandwidth parameters for signals similar to the recorded dolphin clicks.

3 Theoretical study of the practical estimation of the parameters of a click

In this section, we review different methods to estimate, in practice, the parameters of a click presented above as well as some problems encountered. A numerical estimate of these methods is provided in section 4.

3.1 Estimation of the frequency of a click

Click frequency is not something easy to define or measure. One can estimate f_c , f_p by calculating the spectrum, by autocorrelation or by the number of sign changes of the waveform or if we compare the signal to a Gabor wavelet, estimate which f_0 gives the best fit.

3.1.1 Frequency estimation using the spectrum

The estimation of f_p or f_c is classically done by the (approximate) calculation of the spectrum of the signal, in general by a fast Fourier transform (FFT). f_p is then the frequency corresponding to the maximum energy of the spectrum and f_c is the average of the energy-weighted frequencies in each of these frequencies. But, in practice, this method comes up against several difficulties, which we will analyze in the next paragraphs.

Spectrums with several modes The spectra of the clicks recorded at Puyuhuapi are diverse (see figure 3) and can present various more or less strong peaks. They are thus quite different from a Gabor wavelet. The estimate of f_c, which is an average value of the frequencies present in the spectrum is thus difficult for a multimodal spectrum and can have a large uncertainty. There seems to be a whole range of spectra with peak frequencies around of 130 kHz and a whole range with peak frequencies around 170 kHz and, for these clicks, there is a hole in the spectrum around 150 kHz.

The problem of replicas Another important problem for the measurement of the parameters described previously is the very frequent presence of signal replicas, after a few μs. Figure 4 shows two clicks of dolphins recorded in the Puyuhuapi channel in May 2021, where replicas clearly appear i.e. a signal close to a Gabor wavelet that repeats, sometimes attenuated, after a time τ. It is not very clear if these replicas come from two separate emissions from the animal, propagative bounces in its head or whether they come from bounces signals on the surface of the water, the bottom of the fjord or on the device. The 'time delay of arrival' (TDOA) are the order of a few μs between the signal and its replica, which gives course differences of a few centimeters, which which is compatible with internal or external rebounds. The presence of internal bounces or double production of clicks may be a way of improving the signal produced in certain species of dolphins (Lammers and Castellote 2009; de Bruin and Kamminga 2001). A lot of clicks recorded in the Puyuhuapi channel contain one or more replicas.

In this case, we can modelize the signal containing a replica as $x(t) = g(t) + a\ g(t-\tau)$ where τ is the delay time of the replica, a is a real coefficient between -1 et 1 representing an attenuation and g is a Gabor wavelet.

We saw in section 2.2.2 that the indicators f_p (peak frequency) and f_c (centroid frequency) are good indicators of the frequency f_0 of the Gabor wavelet. But in the case of the presence of one or more aftershocks, we will see that these two indicators are strongly degraded. The Fourier transform of x is $X(f) = G(f) \times (1 + ae^{-2i\pi f\tau})$ where G is the Fourier transform of the Gabor wavelet g. The modulus of the coefficient $1 + \ ae^{-2i\pi f\tau}$ is a function of period $\frac{1}{\tau}$ and therefore, in the spectrum, oscillations of period $\frac{1}{\tau}$ appear. An example is given in Figure 5 where the replica arrives 200 μs after the signal, which corresponds to a path difference of approximately 30 cm between the signal and its replica and gives an oscillation of the spectrum at 5 kHz.

In the case of figure 5, it is difficult to accurately measure the peak frequency thanks to the spectrum because of the presence of the replica. And typically, we will have an uncertainty of the order of $\frac{1}{\tau}$ for the estimation of the frequency peak (Wiersma 1982). For the centroid frequency of a Gabor wavelet with replica, a similar phenomenon appears. It can be shown that:

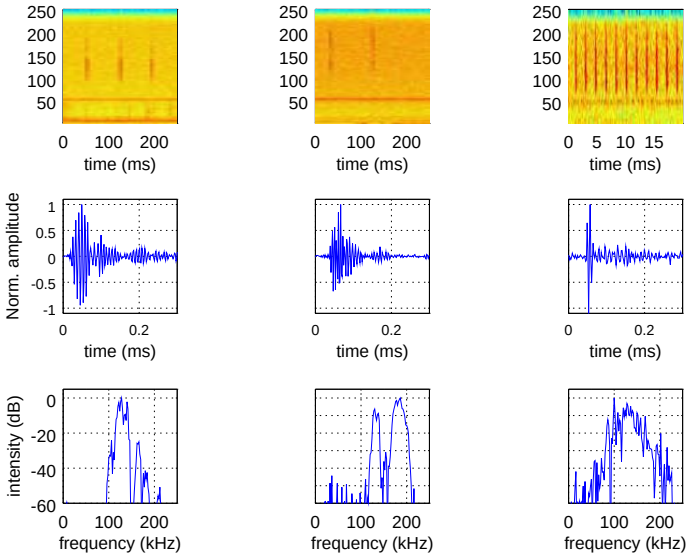

Figure 3: Three clicks from the Puyuhuapi data set. Left : On the left, a typical click of the data set with a frequency peak around 135 kHz. In the center, a click at higher frequency, around 180 kHz. On the right, a click from of a buzz. Top: Top: spectrogram of the signal with an FFT on 2^{10} points (with the exception of the spectrogram right, 2^7 points), blackman window, 50% overlap. Middle : zoom on the normalized waveform of the click located in the center of the spectrogram. Bottom : spectrum of the top click with normalized intensity (FFT of $2^9 = 512$ points i.e. 1 ms of the signal), centered on the detection.

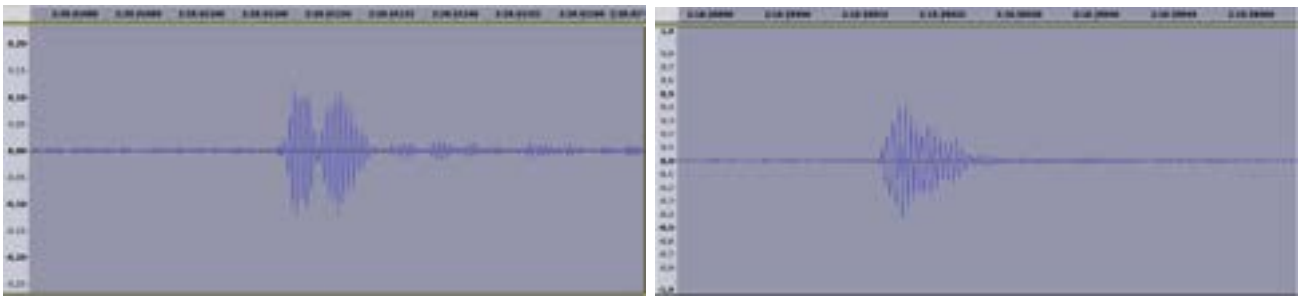

Figure 4: Two waveform dolphin clicks. The left click clearly shows a replica 100 μs after the first sign. The right click seems to present several replicas, possibly two, a few μs after the first signal. We can also note the presence of very weak and diffuse replicas after the first well marked aftershocks

$$f_c = f_0 - \frac{\frac{a\tau}{\pi T^2} e^{-\tau^2/2T^2} \sin(2\pi\tau f_0)}{1 + a^2 + 2a\ e^{-\tau^2/2T^2} \cos(2\pi\tau f_0)}$$

Proof is given in annex 6. In this case, f_c is not necessarily an unbiased estimator of f_0 and figure 6 presents the relative errors between these estimators and the value of f_0 for Gabor wavelets.

We note, however, that the centroid frequency f_c is always a better approximation of f_0 than the peak frequency f_p. In particular, as soon as $\frac{\tau}{T}$ is greater than 3, which corresponds to a very clear separation between the first signal and the replica, the centroid frequency is a good approximation of f_0.

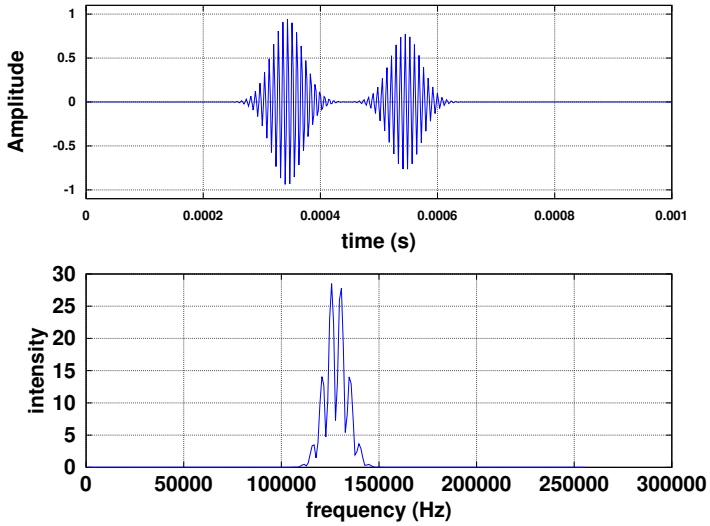

Figure 5: Top : Waveform of a signal composed of a Gabor wavelet type click and a replica separated by $\tau = 200\mu s$. Bottom : The spectrum is composed of the Gaussian centered at f_0 and periodic variations which are superimposed, of period $\frac{1}{\tau} = 5$ kHz

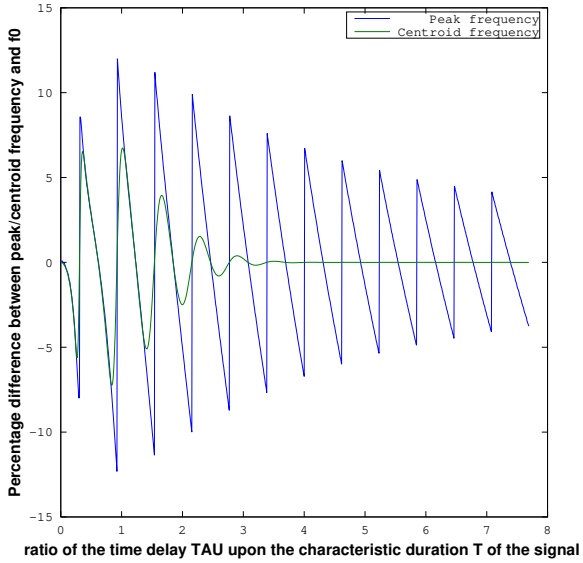

Figure 6: Estimation of the relative error between f_0 and the values f_c (green) and f_p (blue) for a Gabor wavelet followed by a replica after a time τ : $x(t) = g(t) + a\ g(t-\tau)$ with $g(t) = A\ e^{-\frac{(t-t_0)^2}{T^2}}\ cos(2\pi f_0(t-t_0)+\phi)$. In abscissa, we put the ratio $\frac{\tau}{T}$.

3.1.2 Frequency estimation by means of an autocorrelation of the signal

Another way to calculate the fundamental frequency of a periodic signal is to do an autocorrelation of this one (Mellinger and Clark 1997; Malige et al. 2020): $C(r) = lim_{T\to+\infty}\ \frac{1}{T}\int_{-T/2}^{T/2} s(t)s^*(t+r)dt$ where s^* is the complex conjugate of s. A Gabor wavelet is not a periodic signal but in the case of âpolycyclicâ signals, with a high quality factor, i.e. where the oscillation of period $T_0 = 1/f_0$ is well marked, which is the case for the clicks of coastal dolphins present in Chile, we can use $C_s(r) = lim_{T\to+\infty}\ \int_{-T/2}^{T/2} s(t)s^*(t+r)dt$. The theoretical calculation of this function, for a Gabor wavelet g is given in appendix 6 :

$$C_g(r) = \frac{1}{2}\sqrt{\frac{\pi}{2}}A^2T\ e^{-\frac{r^2}{2T^2}}\ [cos(2\pi f_0 r) + cos(2\phi)e^{-2\pi^2 {f_0}^2 T^2}] \simeq \frac{1}{2}\sqrt{\frac{\pi}{2}}A^2T\ e^{-\frac{r^2}{2T^2}}\ cos(2\pi f_0 r)$$

Therefore, the first strictly positive maximum of the autocorrelation function is for $r \simeq \frac{1}{f_0}$ which allows us to estimate f_0. Thus, for each click, we can calculate a discrete version of this autocorrelation function $C_{g,T_{\text{señal}},T_s}(r) = \sum_{n=0}^{\lfloor T_{\text{señal}}/T_s \rfloor} s(nT_s)s(nT_s + r)$ where $T_{\text{señal}}$ is the signal duration time and T_s is the sampling time ($T_s = \frac{1}{f_s}$ where f_s is the sampling frequency ($f_s = 512$ kHz for the Puyuhuapi experiment). The first maximum of this function after zero gives us an estimate of $\frac{1}{f_0}$. However, the sampling frequency is too low here, the discretization in time too coarse, for this method to give us good results, as we will see in section 4. Anyway, even if we had a good sampling frequency, the replicas of the signal can also degrade the estimation of f_0. The autocorrelation function $C_x(r)$ of the signal $x(t)$ (Gabor wavelet with replica) is:

$$C_x(r) = (1 + |a|^2)C_g(r) + aC_g(r + \tau) + aC_g(r - \tau)$$

The new autocorrelation function therefore consists of the curve of C_g to which are added the same curved but shifted by $\pm\tau$ (the delay time of the replica) and attenuated. If τ is large compared to T, these three curves will be quite distinct and the first maximum after zero will still be a good estimator of $1/f_0$. But if τ is low these three curves can be superimposed and we then have a problem when calculating the maximum of this function, which is no longer a good estimator of $1/f_0$.

3.1.3 Frequency estimation thanks to the changes of signs of the waveform

A third way to estimate the frequency f_0 is to count the number of pseudo-periods of the waveform for a given time. Practically, f_0 is calculated as the number of sign changes of the signal during a given time divided by twice the given time. This method is implemented in the C-POD device, without the code used is public (Tregenza 2014). This method seems good when there is little noise but changes in signs from the noise can complicate the estimation.

3.1.4 Frequency estimation by fitting a wavelet or several wavelets

Finally, a last way to calculate f_0 is to fit a Gabor wavelet to our signal. This can be done, for example, by a method of the Levenberg-Marquardt non-linear regression type (âleasqrâ function in OCTAVE language) that fits a type of function to a data set (Kamminga et al. 1996). This adjustment, for each click allows us to find the values of t_0, A, T, f_0 and ϕ. The precision of these adjustments is studied thanks to to the numerical tests of section 4.

3.2 Estimation of Δt and Δf

The values of Δt and Δf are computed by the formulas of section 1.2.

3.2.1 Problem of the estimation of Δt and Δf in the case of a replica

In the case of the presence of a replica (or several), the values of Δt and Δf are modified, as well as the uncertainty product, which is no longer equal to $\frac{1}{4\pi}$ (de Bruin and Kamminga 2001). We can calculate the following formulas (to simplify the calculations, we took $t_0 = 0$, which does not change the values of Δt and Δf) :

$$(\Delta t)^2 = \frac{t_c^2 + \frac{T^2}{4} + a^2((t_c - \tau)^2)\ + (2t_c^2 - 2t_c\tau + \tau^2/2)a\ cos(2\pi f_0\tau)e^{-\frac{\tau^2}{2T^2}}}{(1 + a^2) + 2a\ cos(2\pi f_0\tau)e^{-\frac{\tau^2}{2T^2}}}$$

where $t_c \simeq \tau\frac{a^2 + a\ cos(2\pi f_0\tau)e^{-\frac{\tau^2}{2T^2}}}{1 + a^2 + 2a\ cos(2\pi f_0\tau)e^{-\frac{\tau^2}{2T^2}}}$

$$(\Delta f)^2 = (f_0 - f_c)^2 + \frac{1}{4\pi^2T^2} - \frac{a\tau}{\pi T}\frac{cos(2\pi f_0)\frac{\tau}{\pi^2T^3} + 2sin(2\pi f_0)\frac{f_0 - f_c}{T}}{1 + a^2 + 2acos(2\pi f_0\tau)}$$

It should be noted that these formulas are not very easy to simplify and depend in a complicated way on the parameters t_0, T, a, τ.

3.2.2 Uncertainty product in the case of a replica

In the case of a replica, using the formulas given in the previous paragraph, we calculated the uncertainty product depending on the ratio τ/T. We see that, in this curve, very similar to the curve presented in de Bruin and Kamminga (2001), the uncertainty product is no longer equal to $1/4\pi$ but exhibits oscillations when τ/T is the order of 1 to 3. For a juvenile harbor porpoise (*Phocoena phocoena*), de Bruin and Kamminga (2001) estimate that the value of τ/T coincides with the first local minimum (in our figure, around $\tau/T = 1.2$). They attribute the response to an internal reflection of the sound in the animal.

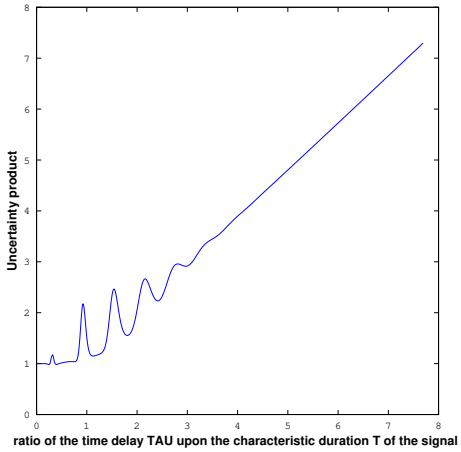

Figure 7: Uncertainty product (multiplied by 4π) in term of τ/T.

For the clicks that we have recorded, we will try to measure the product of uncertainty and also see to what point on the curve (minimum or not) does this correspond to.

4 Numerical tests

4.1 Numerical tests for a noisy Gabor wavelet

The five ways to estimate the peak frequency presented in section 3.1 have been tested on simulated clicks numerically, using a dedicated OCTAVE program: we have generated many noisy Gabor wavelets ($N = 100000$) then we measured the frequency f_0 of the Gabor wavelet in various ways, which we compare with the exact value of f_0 . The noisy wavelets are of the form

$$x(t) = A\ e^{-\frac{(t-t_0)^2}{T^2}}\ cos(2\pi f_0(t-t_0)+\phi) \quad + \quad n(t) \tag{5}$$

The parameters chosen were the following: $A = 0.8 + 0.4X_{[0;1]}$ where $X_{[0;1]}$ is the random variable of distribution continuous uniform on the interval $[0; 1]$. Similarly, the wavelet frequency is $f_0 = 125000kHz \times (0.98 + 0.04X_{[0;1]})$, the average date of the wavelet is $t_0 = 0.00025 + 0.0002X_{[0;1]}$ (in seconds), the characteristic time of duration is $T = 0.00004 + 0.00002X_{[0;1]}$ (in seconds), phase shift $\phi = 2\pi X_{[0;1]}$. We then added a noise Gaussian $n(t)$ to this signal with various intensities. The created function is then sampled at 512 kHz. The signal typical that we obtain is represented in figure 8. The results of the estimations are presented in figure 9.

4.1.1 Frequency estimation

For each of the signals of the form of figure 8, the frequency f_0 of this signal was measured by various methods, as presented in section 3.1 : the peak frequency of the spectrum, the centroid frequency, the autocorrelation of the signal, the number of sign changes of the waveform and the adjustment of a Gabor wavelet. The signal-to-noise ratio ($SNR \simeq 10\ log(\frac{E_{signal}}{E_{bruit}})$) was also estimated for each of the signals. Then we represented the error, in percentage, made during the estimation of fo by each of the methods, as a function of the SNR.

We clearly see, in the figure 9, that the estimate of f_0 is not at all correct by an autocorrelation method, essentially because of the low sampling frequency, compared to the frequency f_0. The methods by maximum or average of the

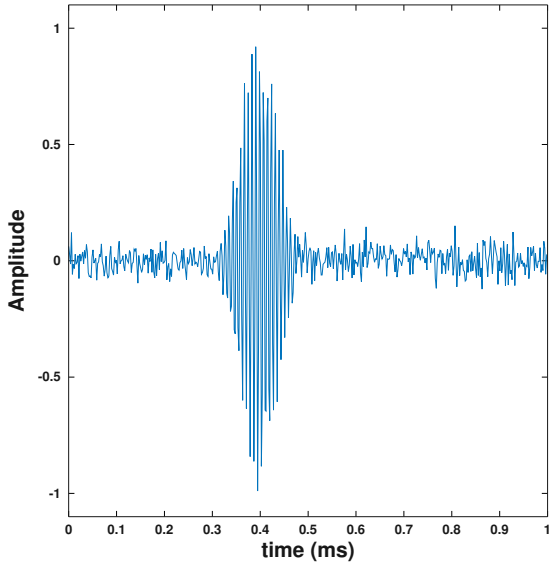

Figure 8: Example of a noisy Gabor wavelet, with the parameters given in the text above. The Gaussian noise has a standard deviation of 0.05.

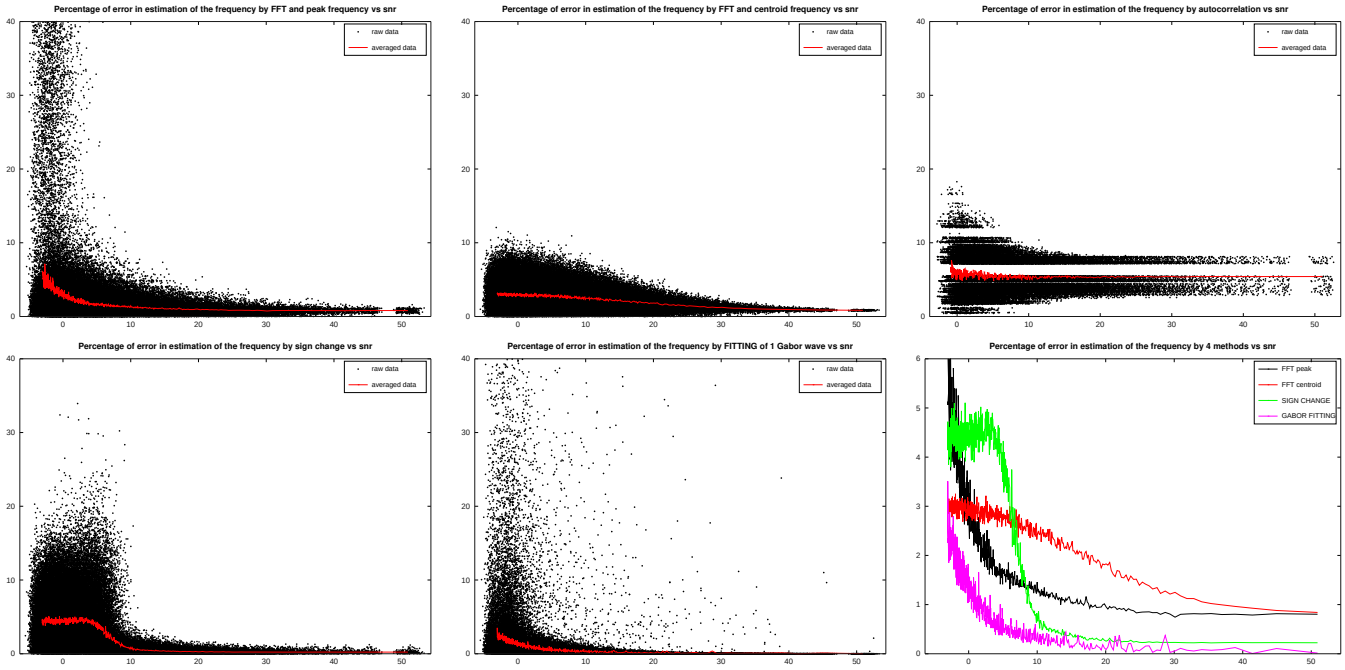

Figure 9: Percentage of error on parameter f_0 as a function of signal to noise (in dB). In black, the errors, in percentage, on the estimate of f_0 for the 10000 synthesized clicks (estimate with the maximum f_p of the FFT, with the centroid frequency f_c using the FFT, with an autocorrelation of the signal, with the changes of sign, with the adjustment of a Gabor wavelet). In red, the average value for each noise level. The bottom right figure compares the means of the figures in the left and center columns.

FFT (frequency peak or centroid) are not very good either and reach a level, independent of the noise, around 1%, as can also be seen in figure 6. The change of sign method is not very good in a noisy context. C-PODs, which use this method are therefore probably not very robust to estimate the frequency in a noisy context. seems to be the fit by a Gabor wavelet.

4.1.2 Duration estimation

Similarly, we measured the various values of the duration of a click (duration -10dB, duration -20dB, rms duration, adjustment by Gabor wavelet) and we compared it to the theoretical value of the Gabor wavelet. In this case, the duration 'rms' seems very sensitive to noise and generally gives poor results. The estimation of the parameter T seems again better by fitting a Gabor wavelet.

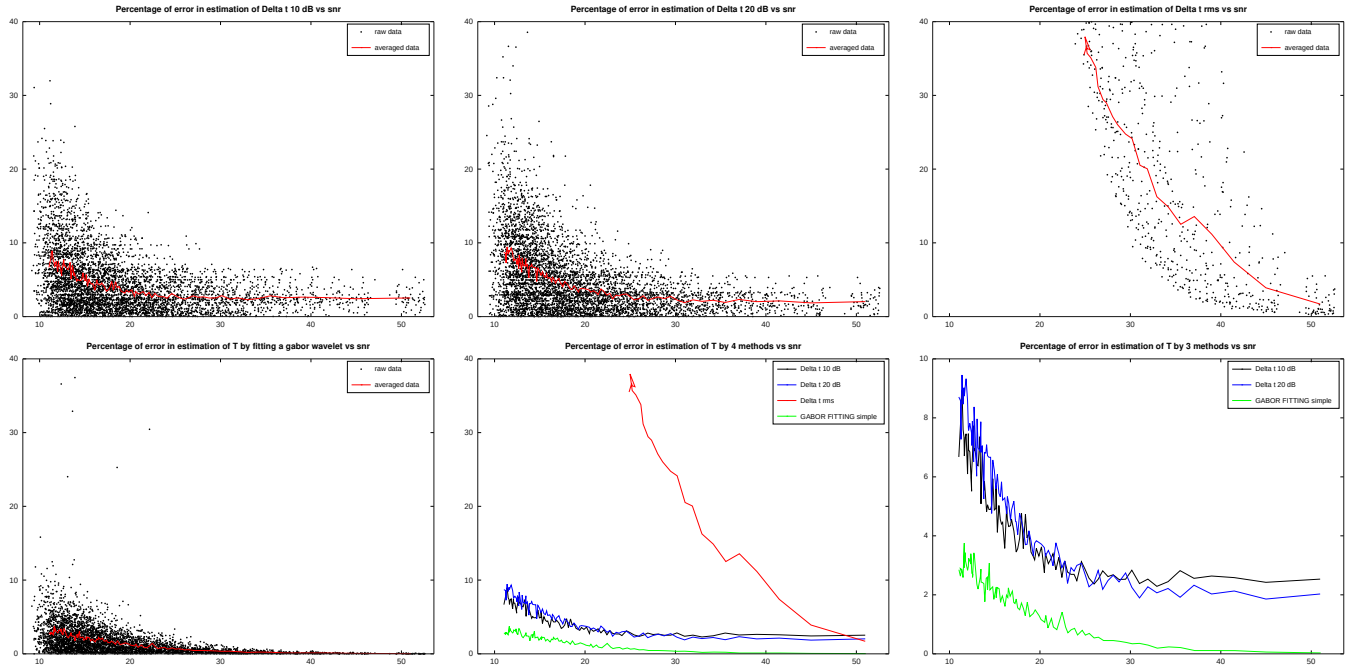

Figure 10: Percentage of error on the estimation of the parameter T according to the signal to noise (in dB). In black, the errors, in percentage, on the estimate of T for 10000 synthesized clicks (estimate with duration -10dB, duration -20dB, rms duration, Gabor wavelet adjustment). In red, the average value for each noise level. The figures at the bottom center and right compare the means of the other 4 figures.

4.1.3 Bandwidth estimation

Similarly, we measured the various values of the frequency band of a click ($\Delta f_{-3\,dB}$ -3dB, $\Delta f_{-10\,dB}$, Δf_{rms} and the value of T by Gabor wavelet adjustment) and we compared these values with the theoretical value (which depends of T). In this case, the 'rms' frequency band seems very sensitive to noise and generally gives poor results. The estimation of the parameter T seems there still better by fitting a Gabor wavelet.

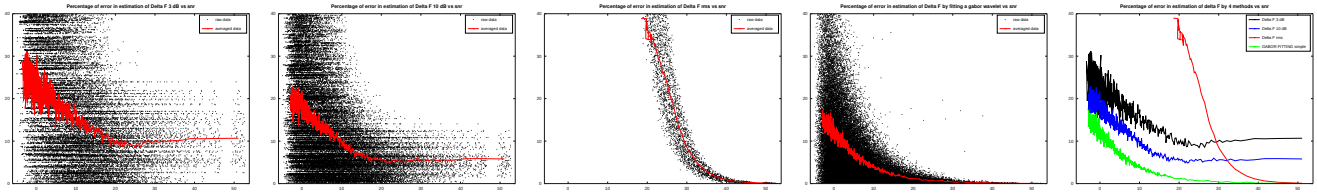

Figure 11: Percentage of error on the estimation of the parameter T through the frequency bands in as a function of signal to noise (in dB). In black, the errors, in percentage, on the estimate of T for 10000 clicks synthesized (estimate with -10dB duration, -20dB duration, rms duration, Gabor wavelet adjustment). In red, the average value for each noise level. Figures at bottom center and right compare means of the other 4 figures.

4.2 Other numerical tests

It is quite normal that fitting a Gabor wavelet to a noisy Gabor wavelet gives good results. We therefore tried to make the same measurements for three other categories of signal, more or less distant of a Gabor wavelet: - A cosine multiplied by a rectangular gate (function $\Pi_{[t_0-T;t_0+T]}$ which equals 1 in this interval and zero elsewhere).

$$x(t) = A\ cos(2\pi f_0(t-t_0)+\phi) \times \Pi_{[t_0-T;t_0+T]} \quad + \quad n(t) \tag{6}$$

- distorted and noisy Gabor wavelets (we multiply the Gabor wavelet by an affine function equal to 1 in t_0).

$$x(t) = A\ e^{-\frac{(t-t_0)^2}{T^2}}\ cos(2\pi f_0(t-t_0)+\phi) \times (1+\frac{t-t_0}{T}) \quad + \quad n(t) \tag{7}$$

- Gabor wavelet with replica :

$$x(t) = A\ e^{-\frac{(t-t_0)^2}{T^2}}\ cos(2\pi f_0(t-t_0)+\phi) + a\ A\ e^{-\frac{(t-t_0-\tau)^2}{T^2}}\ cos(2\pi f_0(t-t_0-\tau)+\phi) \quad + \quad n(t) \tag{8}$$

In the latter case, the delay τ and the attenuation a follow the following laws: $\tau = 0.00005 + 0.0002X_{[0;1]}$ (in seconds) and $a = 0.6 + 0.4X_{[0;1]}$. The results are presented in figure 12. We see that for the first three types of signals, we have similar error estimates, which seems to indicate the robustness of the estimate of these errors, for signals that can be quite different. It should be noted that the centroid frequency is not very good in case 2 (sine multiplied by a gate). This type of signal presents high frequencies (due to the discontinuity of the "gate" function) which can perhaps distort the estimation of the frequency by an average. In the case of a wavelet with replica, the errors are globally larger.

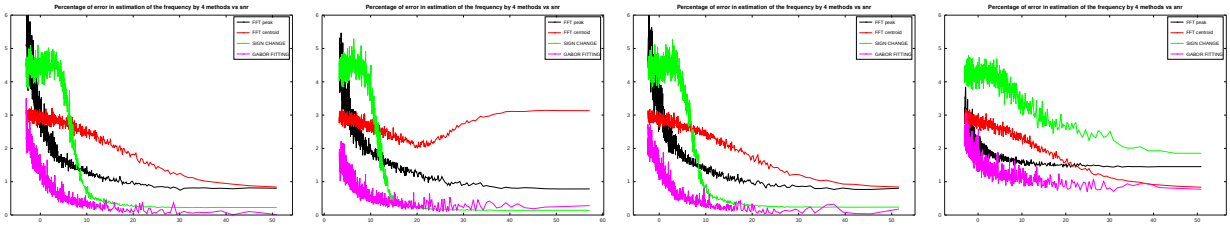

Figure 12: Percentage of error as a function of signal to noise (in dB) for different types of signals: Up to left, for a Gabor wavelet. Top right for a sine multiplied by a gate. Bottom left, for a distorted Gabor wavelet (multiplied by an affine function). Bottom left for a Gabor wavelet with reply.

4.3 Sampling influence

We also measured the influence of sampling on the previous measurements. Indeed, a sampling at 512 kHz is quite 'low', as we have seen for example for autocorrelation measurements. A sampling different will not change the properties of the spectrum (Patris et al. 2019) but on the other hand it can have an influence on the adjustment of a Gabor wavelet. To measure this influence, we measured the frequency of 20000 synthetic clicks (noisy Gabor wavelets) in 5 different ways : by the peak frequency, by the centroid frequency, by the adjustment of a gaborette to the signal sampled at 512 kHz, by the adjustment of a gaborette to the same signal theoretical with a sampling at 2048 kHz, by adjusting a gaborette to the signal at 512 kHz to which we apply the interp function under Octave to digitally oversample it by a factor of 4. The results are in the figure 13. The best methods of measuring the frequency f_0 are that of adjusting a Gabor wavelet to the signal or to a signal with a higher sampling of the theoretical signal (inaccessible in practice). These methods seem better than oversampling our signal using Octave, which gives results similar to measurements by the peak frequency and the centroid frequency.

5 Conclusions

The "frequency" of a click is a concept that can have several meanings. In a classification context, it is important to choose a definition that will allow us to separate the species and therefore to have the lowest uncertainty in the measurments. The measurement of the âfrequencyâ of a dolphin click by change of signs and by autocorrelation does not seem very interesting (especially in the case of sampling at 512 kHz and in a noisy context). Fitting a Gabor

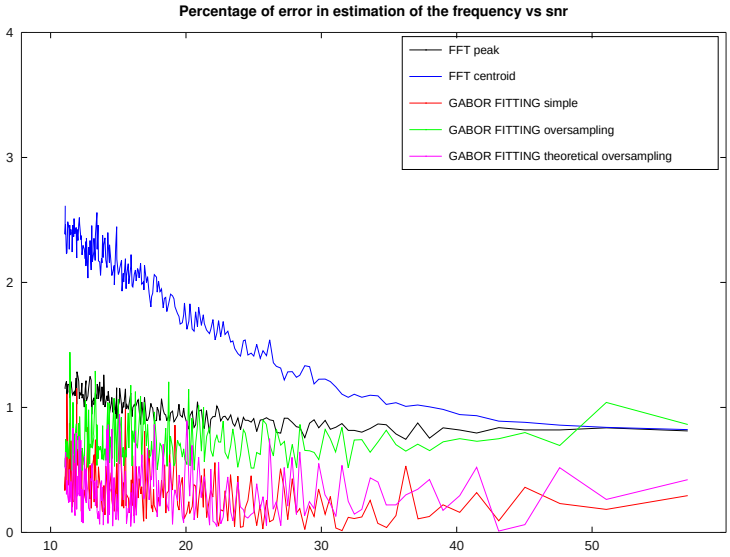

Figure 13: Percentage error as a function of signal to noise (in dB) for different ways of measuring f_0 : by the peak frequency (black), by the centroid frequency (blue), by the adjustment of a gaborette to the sampled signal at 512 kHz (red), by adjusting a gaborette to the same theoretical signal with a sampling at 2048 kHz (pink), by adjusting a gaborette to the 512 kHz signal to which the interp function is applied under Octave to digitally oversample it by a factor of 4 (green)

wavelet seems to be more accurate than calculating a peak or average frequency. We therefore proposes to adjust a Gabor wavelet to the recorded clicks.

6 Annex : Proofs

6.1 General formulas

We give the following form (without proofs), containing classical integrals. Note that, in these formulas, a is homogeneous to a squared frequency.

$\int_{-\infty}^{\infty} e^{-at^2} dt = \sqrt{\frac{\pi}{a}}$

$\int_{-\infty}^{\infty} te^{-at^2} dt = 0$ (by parity)

$\int_{-\infty}^{\infty} t^2 e^{-at^2} dt = \frac{1}{2a}\sqrt{\frac{\pi}{a}}$

$\int_{-\infty}^{\infty} cos(2\pi f_0 t)\ e^{-at^2} dt = \sqrt{\frac{\pi}{a}}\ e^{-\frac{\pi^2 f_0^2}{a}}$

$\int_{-\infty}^{\infty} sin(2\pi f_0 t)\ e^{-at^2} dt = 0$ (by parity)

$\int_{-\infty}^{\infty} t\ sin(2\pi f_0 t)\ e^{-at^2} dt = \frac{\pi f_0}{a}\sqrt{\frac{\pi}{a}}\ e^{-\frac{\pi^2 f_0^2}{a}}$

$\int_{-\infty}^{\infty} t^2\ cos(2\pi f_0 t)\ e^{-at^2} dt = \frac{1}{2a}\sqrt{\frac{\pi}{a}}\ e^{-\frac{\pi^2 f_0^2}{a}}\ (1 - \frac{4\pi f_0^2}{a})$

Remark : in the polycyclic case and for $a = T^2$, the last 4 integrals will be considered as close to zero because the term $e^{-\pi^2 T^2 f_0^2}$ is very small.

6.2 Proofs

We use the formulas above in many calculations, without necessarily recalling them.

6.2.1 Complex Gabor wavelet

In this section, we present the results of table 1, for the column of the complex Gabor wavelet $\underline{g}(t) = Ae^{-\frac{(t-t_0)^2}{T^2}}\ e^{2i\pi f_0(t-t_0)+i\phi}$.

Fourier transform The Fourier transform of the complexe Gabor wavelet $\underline{g}(t) = Ae^{-\frac{(t-t_0)^2}{T^2}}\ e^{2i\pi f_0(t-t_0)+i\phi}$ is $\underline{G}(f) = \int_{-\infty}^{\infty} \underline{g}(t)e^{-2i\pi ft}dt$.

Therefore, $\underline{G}(f) = \int_{-\infty}^{\infty} Ae^{-\frac{(t-t_0)^2}{T^2}}\ e^{2i\pi f_0(t-t_0)+i\phi}e^{-2i\pi ft}dt = Ae^{i\phi}\int_{-\infty}^{\infty} e^{-\frac{u^2}{T^2}}\ e^{2i\pi f_0 u}e^{-2i\pi f(u+t_0)}du =$

$= Ae^{i\phi}e^{-2i\pi ft_0}\int_{-\infty}^{\infty} e^{-\frac{u^2}{T^2}+2i\pi(f_0-f)u}du = Ae^{i\phi}e^{-2i\pi ft_0}\int_{-\infty}^{\infty} e^{-\frac{1}{T^2}(u^2+2i\pi T^2(f-f_0)u)}du$

$= Ae^{i\phi}e^{-2i\pi ft_0}\int_{-\infty}^{\infty} e^{-\frac{1}{T^2}((u+i\pi T^2(f-f_0))^2+\pi^2T^4(f-f_0)^2)}du$

$= Ae^{i\phi}e^{-2i\pi ft_0}e^{-\pi^2T^2(f-f_0)^2}\int_{-\infty}^{\infty} e^{-\frac{1}{T^2}((u+i\pi T^2(f-f_0))^2}du$

$= Ae^{i\phi}e^{-2i\pi ft_0}e^{-\pi^2T^2(f-f_0)^2}\int_{-\infty}^{\infty} e^{-\frac{u^2}{T^2}}du$ (Residue theorem)

$= AT\sqrt{\pi}\ e^{-2i\pi ft_0+i\phi}e^{-\pi^2T^2(f-f_0)^2}$

Energy $E = \int_{-\infty}^{\infty}|\mathrm{g}(t)|^2dt = A^2\int_{-\infty}^{\infty} e^{-\frac{2(t-t_0)^2}{T^2}}dt = A^2\int_{-\infty}^{\infty} e^{-\frac{2u^2}{T^2}}du = A^2T\sqrt{\frac{\pi}{2}}$

Average date The average date t_c is computed as the moment of order 1 of time considering $|\mathrm{g}(t)|^2$ as a probability density.

$t_c = \frac{\int_{-\infty}^{\infty} t|\mathrm{g}(t)|^2dt}{\int_{-\infty}^{\infty}|\mathrm{g}(t)|^2dt} = \frac{1}{E}\int_{-\infty}^{\infty} tA^2e^{-\frac{2(t-t_0)^2}{T^2}}dt = \frac{A^2}{E}\int_{-\infty}^{\infty}(u+t_0)e^{-\frac{2u^2}{T^2}}du = \frac{A^2}{E}\int_{-\infty}^{\infty} t_0\ e^{-\frac{2u^2}{T^2}}du$ (by parity)

$= \frac{A^2}{E}t_0\int_{-\infty}^{\infty} e^{-\frac{2u^2}{T^2}}du = t_0$

Duration at -10dB and -20 dB The duration at -10 dB, denoted $\Delta t_{-10\ dB}$, is calculated as the duration during which the envelope of g_(t) is greater than the maximum value of g minus -10 dB. This translates to 20 $log(\frac{envelope\ of\ \mathrm{g}(t)}{maximum\ of\ \mathrm{g}(t)}) > -10$

Thus $log(\frac{|A|\ e^{-\frac{(t-t_0)^2}{T^2}}}{|A|}) > -\frac{1}{2}$

Thus $-\frac{(t-t_0)^2}{T^2} > -\frac{ln(10)}{2}$

Thus $|t-t_0| < \sqrt{\frac{ln(10)}{2}}T$

Thus $\Delta t_{-10\ dB} = \sqrt{2ln(10)}T$

similarly, $\Delta t_{-20\ dB} = \sqrt{4ln(10)}T$

Duration 'rms' The duration 'rms', denoted Δt is the moment of order 2 of the temporal density and is equal to $(\Delta t)^2 = \frac{\int_{-\infty}^{+\infty}(t-t_c)^2|\mathrm{g}(t)|^2dt}{\int_{-\infty}^{+\infty}|\mathrm{g}(t)|^2dt}$

Thus $(\Delta t)^2 = \frac{1}{E}\int_{-\infty}^{+\infty}(t-t_0)^2|\mathrm{g}(t)|^2dt = \frac{A^2}{E}\int_{-\infty}^{+\infty}(t-t_0)^2e^{-\frac{2(t-t_0)^2}{T^2}}dt = \frac{A^2}{E}\int_{-\infty}^{+\infty} u^2e^{-\frac{2u^2}{T^2}}du = \frac{A^2}{E}\sqrt{\frac{\pi T^2}{2}}\frac{T^2}{4} = \frac{T^2}{4}$

and then $\Delta t = \frac{T}{2}$

Peak frequency The peak frequency is the frequency for which the modulus of the Fourier transform is maximal. In the case of a complex Gabor wavelet, $|\underline{\mathrm{G}}(f)| = AT\sqrt{\pi}e^{-\pi^2T^2(f-f_0)^2}$ and its maximum is reached for $f_p = f_0$.

Centroïde frequency The centroid frequency is calculated as the moment of order 1 of the frequencies, considering $|\underline{\mathrm{G}}(f)|^2$ as a density.

$f_c = \frac{\int_{-\infty}^{\infty} f|\underline{\mathrm{G}}(f)|^2df}{\int_{-\infty}^{\infty}|\underline{\mathrm{G}}(f)|^2df} = \frac{1}{E}\int_{-\infty}^{\infty} fA^2T^2\pi e^{-2\pi^2T^2(f-f_0)^2}df$ (Parseval theorem)

$= \frac{A^2T^2\pi}{E}\int_{-\infty}^{\infty}(u+f_0)e^{-2\pi^2T^2u^2}du$ (changing the variable $f = u+f_0$)

$= f_0\frac{A^2T^2\pi}{E}\int_{-\infty}^{\infty} e^{-2\pi^2T^2u^2}du$ (by parity)

$= f_0\frac{A^2T^2\pi}{E}\sqrt{\frac{\pi}{2\pi^2T^2}} = f_0\frac{A^2T\sqrt{\pi}}{\sqrt{2}E} = f_0$

Bandwidth at -3 dB and -10 dB The bandwidth at -3 dB, denoted $\Delta f_{-3\ dB}$, is calculated as the length of the frequency range over which the envelope of $underbarG(f)$ is greater than the maximum value of S minus -3 dB, which is an approximation of the fact that $\frac{envelope\ of underbarG(f)}{max\quad \underline{\mathrm{G}}(f)} > \frac{1}{\sqrt{2}}$

Thus $\frac{AT\sqrt{\pi}\ e^{-\pi^2T^2(f-f_0)^2}}{AT\sqrt{\pi}} > \frac{1}{\sqrt{2}}$

Thus $-\pi^2T^2(f-f_0)^2 > ln(\frac{1}{\sqrt{2}})$

Thus $\pi^2T^2(f-f_0)^2 < \frac{ln(2)}{2}$

Thus $|f-f_0| < \frac{1}{\pi T}\sqrt{\frac{ln(2)}{2}}$

Thus $\Delta f_{-3\ dB} = \frac{1}{\pi T}\sqrt{2ln(2)}$

Similarly, $\Delta t_{-10\ dB} = \frac{\sqrt{2ln(10)}}{\pi T}$

Bandwidth 'rms' The rms bandwidth is the second moment associated with the frequency distribution and is equal to $\Delta f = \sqrt{\frac{\int_{-\infty}^{+\infty}(f-f_c)^2|\underline{\mathrm{G}}(f)|^2df}{\int_{-\infty}^{+\infty}|\underline{\mathrm{G}}(f)|^2df}}$

Thus $(\Delta f)^2 = \frac{1}{E}\int_{-\infty}^{+\infty}(f-f_0)^2|\underline{\mathrm{G}}(f)|^2df = \frac{1}{E}\int_{-\infty}^{+\infty}(f-f_0)^2A^2T^2\pi\ e^{-2\pi^2T^2(f-f_0)^2}df = \frac{A^2T^2\pi}{E}\int_{-\infty}^{+\infty} u^2\ e^{-2\pi^2T^2u^2}du$

$= \frac{A^2T^2\pi}{E}\frac{1}{4\pi^2T^2}\sqrt{\frac{\pi}{2\pi^2T^2}} = \frac{1}{4\pi^2T^2}$

Then $\Delta f = \frac{1}{2\pi T}$

Quality factor at -3dB Quality factor at -3dB is $Q_{(3dB)} = \frac{f_c}{\Delta f_{(-3dB)}} = \frac{\pi f_0 T}{\sqrt{2ln(2)}}$

Quality factor 'rms' Quality factor 'rms' is $Q_{rms} = \frac{f_c}{\Delta f} = 2\pi f_0 T$.

Uncertainty product The uncertainty product or duration-bandwidth product is equal to $P_{incert} = \Delta t \times \Delta f$. Then $P_{incert} = \frac{T}{2}\frac{1}{2\pi T} = \frac{1}{4\pi}$

Autocorrelation function The autocorrelation function is defined by $C_s(r) = \int_{-\infty}^{+\infty} s(t)s^*(t+r)dt$

Then, for a complex Gabor wavelet : $C_g(r) = A^2 \int_{-\infty}^{+\infty} e^{-\frac{(t-t_0)^2}{T^2}}\ e^{2i\pi f_0(t-t_0)+i\phi} e^{-\frac{(t+r-t_0)^2}{T^2}}\ e^{-2i\pi f_0(t+r-t_0)-i\phi} dt$

$= A^2 \int_{-\infty}^{+\infty} e^{-\frac{(t-t_0)^2}{T^2}}\ e^{-\frac{(t+r-t_0)^2}{T^2}}\ e^{-2i\pi f_0 r} dt = A^2 e^{-2i\pi f_0 r} \int_{-\infty}^{+\infty} e^{\frac{-u^2-(u+r)^2}{T^2}} du = A^2 e^{-2i\pi f_0 r} \int_{-\infty}^{+\infty} e^{-\frac{1}{T^2}(2u^2+2ur+r^2)} du$

$= A^2 e^{-2i\pi f_0 r} \int_{-\infty}^{+\infty} e^{-\frac{2}{T^2}((u+\frac{r}{2})^2+\frac{r^2}{4})} du = A^2 e^{-2i\pi f_0 r} e^{-\frac{r^2}{2T^2}} \int_{-\infty}^{+\infty} e^{-\frac{2(u+\frac{r}{2})^2}{T^2}} du = A^2 e^{-2i\pi f_0 r} e^{-\frac{r^2}{2T^2}} \int_{-\infty}^{+\infty} e^{-\frac{2v^2}{T^2}} dv$

$= A^2 e^{-2i\pi f_0 r} e^{-\frac{r^2}{2T^2}} \sqrt{\frac{\pi}{2}} T$

6.2.2 Real Gabor wavelet

In this section, we present the calculations of table 1, for the column of the real Gabor wavelet. For these calculations, and for the sake of simplification, we will place ourselves in the case of a "polycyclic" Gabor wavelet, which is the model we use to approximate the clicks of coastal dolphins, c is to say in the case where $\pi^2 f_0^2 T^2$ is large and therefore $e^{-\pi^2 f_0^2 T^2} \simeq 0$.

Fourier transform We want to compute $G(f) = \int_{-\infty}^{\infty} g(t)e^{-2i\pi ft}dt$ where g is the real Gabor wavelet : $g(t) = Ae^{-\frac{(t-t_0)^2}{T^2}}\ cos(2\pi f_0(t-t_0)+\phi)$

Thus, $G(f) = \int_{-\infty}^{\infty} Ae^{-\frac{(t-t_0)^2}{T^2}}\ cos(2\pi f_0(t-t_0)+\phi)e^{-2i\pi ft}dt = A\int_{-\infty}^{\infty} e^{-\frac{u^2}{T^2}}\ cos(2\pi f_0 u+\phi)e^{-2i\pi f(u+t_0)}du$

$= \frac{A}{2}e^{-2i\pi ft_0}\int_{-\infty}^{\infty} e^{-\frac{u^2}{T^2}}[e^{2i\pi f_0 u+i\phi} + e^{-2i\pi f_0 u-i\phi}]e^{-2i\pi fu}du$

$= \frac{A}{2}e^{-2i\pi ft_0}[e^{i\phi}\int_{-\infty}^{\infty} e^{-\frac{u^2}{T^2}}e^{-2i\pi(f-f_0)u}du + e^{-i\phi}\int_{-\infty}^{\infty} e^{-\frac{u^2}{T^2}}e^{-2i\pi(f+f_0)u}du]$

Similarly to the complex case :

$G(f) = \frac{AT\sqrt{\pi}}{2}e^{-2i\pi ft_0}[e^{i\phi}e^{-\pi^2T^2(f-f_0)^2} + e^{-i\phi}e^{-\pi^2T^2(f+f_0)^2}]$

Energy $E = \int_{-\infty}^{\infty}|g(t)|^2dt = A^2\int_{-\infty}^{\infty} e^{-\frac{2(t-t_0)^2}{T^2}}cos^2(2\pi f_0(t-t_0)+\phi)dt = A^2\int_{-\infty}^{\infty} e^{-\frac{2u^2}{T^2}}cos^2(2\pi f_0 u+\phi)du$

$= \frac{A^2}{2}\int_{-\infty}^{\infty} e^{-\frac{2u^2}{T^2}}[1+cos(4\pi f_0 u+2\phi)]du = \frac{A^2}{2}\int_{-\infty}^{\infty} e^{-\frac{2u^2}{T^2}}du + \frac{A^2}{2}cos(2\phi)\int_{-\infty}^{\infty} e^{-\frac{2u^2}{T^2}}cos(4\pi f_0 u)du$

$= \frac{A^2}{2}\sqrt{\frac{\pi}{2}}[T + cos(2\phi)e^{-2\pi^2f_0^2T^2}] \simeq \frac{A^2}{2}\sqrt{\frac{\pi}{2}}T$ because $e^{-2\pi^2f_0^2T^2} \simeq 0$

Average date The average time t_c is calculated as the moment of order 1 of the time, considering $|g(t)|^2$ as a density.

$t_c = \frac{\int_{-\infty}^{\infty} t|g(t)|^2dt}{\int_{-\infty}^{\infty}|g(t)|^2dt} = \frac{1}{E}\int_{-\infty}^{\infty} tA^2e^{-\frac{2(t-t_0)^2}{T^2}}cos^2(2\pi f_0(t-t_0)+\phi)dt = \frac{A^2}{2E}\int_{-\infty}^{\infty}(u+t_0)e^{-\frac{2u^2}{T^2}}[1+cos(4\pi f_0 u+2\phi)]du$

$= \frac{A^2}{2E}\int_{-\infty}^{\infty}(u+t_0)e^{-\frac{2u^2}{T^2}}[1+cos(4\pi f_0 u)cos(2\phi) - sin(4\pi f_0 u)sin(\phi)]du$

$= \frac{A^2}{2E}\int_{-\infty}^{\infty}[t_0e^{-\frac{2u^2}{T^2}}(1+cos(4\pi f_0 u)cos(2\phi)) - ue^{-\frac{2u^2}{T^2}}sin(4\pi f_0 u)sin(\phi)]du$

$= \frac{A^2}{2E}[t_0\ \sqrt{\frac{\pi}{2}}T + t_0\ cos(2\phi)\ \sqrt{\frac{\pi}{2}}Te^{-2\pi^2f_0^2T^2} - sin(2\phi)\pi f_0T^2\sqrt{\frac{\pi}{2}}Te^{-2\pi^2f_0^2T^2}]$

$= t_0 + (t_0\ cos(2\phi) - \pi sin(2\phi)f_0T^2)e^{-2\pi^2f_0^2T^2} \simeq t_0$ car $e^{-2\pi^2f_0^2T^2} \simeq 0$

Duration at -10dB and -20 dB The duration at -10 dB, denoted $\Delta t_{-10\ dB}$, is calculated as the duration during which the envelope of $g(t)$ is greater than the maximum value of g minus -10 dB. However, if we consider that we are in the polycyclic case, the frequency f_0 is large enough to be considered the carrier of the signal and the envelope is the m ême in the real case where complex. We therefore have the same values for the durations at -10dB and -20 dB in the real or complex case.

Duration 'rms' The duration 'rms', denoted Δt is the moment of order 2 of the temporal density and is equal to $(\Delta t)^2 = frac\int_{-\infty}^{+\infty}(t-t_c)^2|g(t)|^2dt\int_{-\infty}^{+\infty}|g(t)|^2dt$. We will assume here that $t_c = t_0$, in accordance with the calculation and approximation above.

Then $(\Delta t)^2 = \frac{1}{E}\int_{-\infty}^{+\infty}(t-t_0)^2|s(t)|^2dt = \frac{A^2}{E}\int_{-\infty}^{+\infty}(t-t_0)^2e^{-\frac{2(t-t_0)^2}{T^2}}(cos(2\pi f_0(t-t_0)+\phi))^2dt =$

$= \frac{A^2}{E}\int_{-\infty}^{+\infty}u^2e^{-\frac{2u^2}{T^2}}(cos(2\pi f_0 u+\phi))^2du = \frac{A^2}{2E}\int_{-\infty}^{+\infty}u^2e^{-\frac{2u^2}{T^2}}(1+cos(4\pi f_0 u+2\phi))du =$

$= \frac{A^2}{2E}[\int_{-\infty}^{+\infty}u^2e^{-\frac{2u^2}{T^2}}du + \int_{-\infty}^{+\infty}u^2e^{-\frac{2u^2}{T^2}}cos(4\pi f_0 u+2\phi)du = \frac{A^2}{2E}[\frac{T^3}{4}\sqrt{\frac{\pi}{2}} + cos(2\phi)\frac{T^3}{4}\sqrt{\frac{\pi}{2}}e^{-2\pi^2f_0^2T^2/2}(1-8\pi f_0^2T^2)]$

$= \frac{T^2}{4}\frac{1+cos(2\phi)e^{-2\pi^2{f_0}^2T^2}(1-8\pi{f_0}^2T^2)}{1+cos(2\phi)e^{-2\pi^2{f_0}^2T^2}}$

Using the approximation $e^{-2\pi^2f_0^2T^2} \simeq 0$, we obtain $(\Delta t)^2 \simeq \frac{T^2}{4}$

Then $\Delta t \simeq \frac{T}{2}$.

Peak frequency The peak frequency is the frequency for which the modulus of the Fourier transform is maximal. In the case of a complex Gabor wavelet, $G(f) = \frac{AT}{2} e^{-2i\pi f t_0}[e^{i\phi} e^{-\pi^2 T^2 (f-f_0)^2} + e^{-i\phi} e^{-\pi^2 T^2 (f+f_0)^2}]$ and its maximum, in frpositive sequences, is reached for $f_p = f_0$.

Centroid frequency, bandwidth at -3 dB and at -10 dB, bandwidth rms, quality factor at -3dB, quality factor "rms ", uncertainty product The centroid frequency is calculated as the moment of order 1 of the frequencies, considering $|G(f)|^2$ as a density. As the function $|G(f)|^2$ is even then $f_c = 0$. But if we want to make sense of the centroid frequency then we can use the analytical signal associated with s. In this case, and in the polycyclic approximation, we have $f_c \simeq f_0$, as in the case of a complex Gabor wavelet. Similarly, the other parameters calculated in the previous section (bandwidth at -3 dB and at -10 dB, rms bandwidth, quality factor e at -3dB, "rms" quality factor, uncertainty product), based on the spectrum of g are equal, if we consider that we are in the polycyclic case.

Autocorrelation function The autocorrelation function is defined by $C_s(r) = \int_{-\infty}^{+\infty} s(t)s^*(t+r)dt$. And so, for a complex Gabor wavelet:

$C_g(r) = A^2 \int_{-\infty}^{+\infty} e^{-\frac{(t-t_0)^2}{T^2}}\ cos(2\pi f_0(t-t_0)+\phi)\ e^{-\frac{(t+r-t_0)^2}{T^2}}\ cos(2\pi f_0(t+r-t_0)+\phi)dt$

$C_g(r) = A^2 \int_{-\infty}^{+\infty} e^{-\frac{u^2}{T^2}}\ cos(2\pi f_0 u+\phi)\ e^{-\frac{(u+r)^2}{T^2}}\ cos(2\pi f_0(u+r)+\phi)du$ changing the variable $u = t - t_0$

$C_g(r) = \frac{A^2}{2} \int_{-\infty}^{+\infty} e^{-\frac{2u^2+2ur+r^2}{T^2}}\ [cos(4\pi f_0 u + \pi f_0 r + 2\phi) + cos(2\pi f_0 r)]du$

$C_g(r) = \frac{A^2}{2} \int_{-\infty}^{+\infty} e^{-\frac{2(u+r/2)^2+r^2/2}{T^2}}\ [cos(4\pi f_0(u+r/2)+2\phi) + cos(2\pi f_0 r)]du$

$C_g(r) = \frac{A^2}{2} e^{\frac{-r^2}{2T^2}} \int_{-\infty}^{+\infty} e^{-\frac{2(u+r/2)^2}{T^2}}\ [cos(4\pi f_0(u+r/2)+2\phi) + cos(2\pi f_0 r)]du$

$C_g(r) = \frac{A^2}{2} e^{\frac{-r^2}{2T^2}} \int_{-\infty}^{+\infty} e^{-\frac{2v^2}{T^2}}\ [cos(4\pi f_0 v + 2\phi) + cos(2\pi f_0 r)]dv$ changing the variable $v = u + r/2$

$C_g(r) = \frac{A^2}{2} e^{\frac{-r^2}{2T^2}} [T\sqrt{\frac{\pi}{2}} e^{-2\pi^2 f_0^2 T^2} cos(2\phi) + T\sqrt{\frac{\pi}{2}} cos(2\pi f_0 r)]$ by parity

$C_g(r) = \frac{A^2 T}{2}\sqrt{\frac{\pi}{2}}\ e^{\frac{-r^2}{2T^2}}\ [cos(2\pi f_0 r) + e^{-2\pi^2 f_0^2 T^2} cos(2\phi)]$

Finaly : $C_g(r) \simeq \frac{A^2 T}{2}\sqrt{\frac{\pi}{2}}\ e^{\frac{-r^2}{2T^2}}\ cos(2\pi f_0 r)$

6.2.3 Real Gabor wavelet with replica

We note $x(t) = g(t) + ag(t-\tau)$ where a is a real number measuring the attenuation of the replica and $tau > 0$ is the delay between the first gaborette and its replica. We recall that $g(t) = Ae^{-\frac{(t-t_0)^2}{T^2}}\ cos(2\pi f_0(t-t_0)+\phi)$

Fourier transform The Fourier transform of a signal with replica is

$X(f) = G(f) + a\int_{-\infty}^{+\infty} g(t-\tau)e^{-2i\pi f t}dt = G(f) + a\int_{-\infty}^{+\infty} g(u)e^{-2i\pi f(u+\tau)}du = G(f) + ae^{-2i\pi f\tau}\int_{-\infty}^{+\infty} g(u)e^{-2i\pi f u}du$

Then $X(f) = G(f) + ae^{-2i\pi f\tau}G(f) = G(f)[1 + ae^{-2i\pi f\tau}]$

Energy $E = \int_{-\infty}^{\infty} |x(t)|^2 dt = \int_{-\infty}^{\infty} |X(f)|^2 df$

Thus $E = \int_{-\infty}^{\infty} |G(f)|^2 |1 + ae^{-2i\pi f\tau}|^2 df$

We have $G(f) = \frac{AT\sqrt{\pi}}{2} e^{-2i\pi f t_0}[e^{i\phi} e^{-\pi^2 T^2 (f-f_0)^2} + e^{-i\phi} e^{-\pi^2 T^2 (f+f_0)^2}]$

In the polycyclic case $|G(f)|^2 \simeq \frac{A^2 T^2 \pi}{4}(e^{-2\pi^2 T^2 (f-f_0)^2} + e^{-2\pi^2 T^2 (f+f_0)^2})$

Thus $E \simeq \frac{A^2 T^2 \pi}{4}\int_{-\infty}^{\infty}(e^{-2\pi^2 T^2 (f-f_0)^2} + e^{-2\pi^2 T^2 (f+f_0)^2})|1 + ae^{-2i\pi f\tau}|^2 df$

Thus $E \simeq \frac{A^2 T^2 \pi}{4}\int_{-\infty}^{\infty}(e^{-2\pi^2 T^2 (f-f_0)^2} + e^{-2\pi^2 T^2 (f+f_0)^2})[1 + a^2 + 2a\ cos(2\pi f\tau)]df$

$E \simeq \frac{A^2 T^2 \pi}{2}[(1+a^2)\int_{-\infty}^{\infty} e^{-2\pi^2 T^2 u^2}du + a\int_{-\infty}^{\infty}(e^{-2\pi^2 T^2 (f-f_0)^2} + e^{-2\pi^2 T^2 (f+f_0)^2})cos(2\pi f\tau)df]$

$E \simeq \frac{A^2 T^2 \pi}{2}[(1+a^2)\sqrt{\frac{\pi}{2\pi^2 T^2}} + a\int_{-\infty}^{\infty} e^{-2\pi^2 T^2 u^2}[cos(2\pi(u+f_0)\tau) + cos(2\pi(u-f_0)\tau)]du]$

$E \simeq \frac{A^2 T^2 \pi}{2}[(1+a^2)\sqrt{\frac{\pi}{2\pi^2 T^2}} + 2a\int_{-\infty}^{\infty} e^{-2\pi^2 T^2 u^2}[cos(2\pi u\tau)cos(2\pi f_0\tau)]du]$

$E \simeq \frac{A^2 T^2 \pi}{2}[(1+a^2)\sqrt{\frac{\pi}{2\pi^2 T^2}} + 2a\ cos(2\pi f_0\tau)\int_{-\infty}^{\infty} e^{-2\pi^2 T^2 u^2}[cos(2\pi u\tau)]du]$

$E \simeq \frac{A^2 T^2 \pi}{2}[(1+a^2)\sqrt{\frac{\pi}{2\pi^2 T^2}} + 2a\ cos(2\pi f_0\tau)\sqrt{\frac{\pi}{2\pi^2 T^2}} e^{-\frac{\pi^2\tau^2}{2\pi^2 T^2}}]$

$E \simeq \frac{A^2 T\sqrt{\pi}}{2\sqrt{2}}[(1+a^2) + 2a\ cos(2\pi f_0\tau)e^{-\frac{\tau^2}{2T^2}}]$

Remark : The energy depends in a non-obvious way on the values of τ and a. We can however note that when τ becomes large compared to T then the energy of the signal is the addition of the energy of two Gabor wavelets, one of which is attenuated 'ee of a relative to the other.

Average date the average time t_c is calculated as the moment of order 1 of the time, considering $|x(t)|^2$ as a density.

$t_c = \frac{\int_{-\infty}^{\infty} t|x(t)|^2 dt}{\int_{-\infty}^{\infty} |x(t)|^2 dt} = \frac{1}{E}\int_{-\infty}^{\infty} t(g(t) + ag(t-\tau))^2 dt = \frac{1}{E}[\int_{-\infty}^{\infty} t(g(t))^2 dt + a^2\int_{-\infty}^{\infty} t(g(t-\tau))^2 dt + 2a\int_{-\infty}^{\infty} tg(t)g(t-\tau)dt]$

$Et_c \simeq t_0\frac{A^2 T\sqrt{\pi}}{2\sqrt{2}} + a^2\int_{-\infty}^{\infty}(u+\tau)(g(u))^2 du + 2aA^2\int_{-\infty}^{\infty} te^{-\frac{(t-t_0)^2}{T^2}}\ cos(2\pi f_0(t-t_0)+\phi)e^{-\frac{(t-\tau-t_0)^2}{T^2}}\ cos(2\pi f_0(t-\tau-t_0)+\phi)dt$

$$Et_c \simeq \frac{A^2T\sqrt{\pi}}{2\sqrt{2}}(t_0+a^2t_0+a^2\tau)+2aA^2\int_{-\infty}^{\infty}(u+t_0)e^{-\frac{u^2+(u-\tau)^2}{T^2}}\ cos(2\pi f_0u+\phi)\ cos(2\pi f_0(u-\tau)+\phi)du$$

$$Et_c \simeq \frac{A^2T\sqrt{\pi}}{2\sqrt{2}}(t_0+a^2t_0+a^2\tau)+aA^2\int_{-\infty}^{\infty}(u+t_0)e^{-2\frac{(u-\tau/2)^2+\tau^2/4}{T^2}}\ [cos(4\pi f_0u-2\pi f_0\tau+2\phi)+\ cos(2\pi f_0\tau)]du$$

$$Et_c \simeq \frac{A^2T\sqrt{\pi}}{2\sqrt{2}}(t_0+a^2t_0+a^2\tau)+aA^2e^{-\frac{\tau^2}{2T^2}}\int_{-\infty}^{\infty}(v+\tau/2+t_0)e^{-\frac{2v^2}{T^2}}\ [cos(4\pi f_0v+2\phi)+\ cos(2\pi f_0\tau)]dv$$

$$Et_c \simeq \frac{A^2T\sqrt{\pi}}{2\sqrt{2}}(t_0+a^2t_0+a^2\tau)+aA^2e^{-\frac{\tau^2}{2T^2}}\ cos(2\pi f_0\tau)\int_{-\infty}^{\infty}(v+\tau/2+t_0)e^{-\frac{2v^2}{T^2}}dv$$

$$Et_c \simeq \frac{A^2T\sqrt{\pi}}{2\sqrt{2}}(t_0+a^2t_0+a^2\tau)+aA^2e^{-\frac{\tau^2}{2T^2}}\ cos(2\pi f_0\tau)(\tau/2+t_0)\frac{T\sqrt{\pi}}{\sqrt{2}} \qquad \text{(by parity)}$$

$$Et_c \simeq \frac{A^2T\sqrt{\pi}}{2\sqrt{2}}(t_0+a^2t_0+a^2\tau+2ae^{-\frac{\tau^2}{2T^2}}cos(2\pi f_0\tau)(\tau/2+t_0))$$

$$t_c \simeq \frac{t_0+a^2t_0+a^2\tau+2a\ cos(2\pi f_0\tau)e^{-\frac{\tau^2}{2T^2}}(t_0+\tau/2)}{(1+a^2)+2a\ cos(2\pi f_0\tau)e^{-\frac{\tau^2}{2T^2}}}$$

Remark : When τ is large in front of T, the average date $t_c \simeq \frac{t_0+a^2(t_0+\tau)}{1+a^2}$is the average (weight 'ee by the energy) of the dates of the two gaborettes.

Duration at -10dB and -20 dB The duration at -10 dB, denoted $\Delta t_{-10\ dB}$, is calculated as the duration during which the envelope of $s(t)$ is greater than the maximum value of s minus -10 dB. This translates to 20 $log(\frac{envelope\ of\ x(t)}{maximum\ of\ x(t)}) > -10$. In the case of a wave with a replica, this calculation is difficult to carry out but we see that this duration will be of the order of a multiple of T. We prefer to use the "rms" duration that we calculate in the next paragraph.

Duration 'rms' The duration 'rms', denoted Δt is the moment of order 2 of the temporal density and is equal to $(\Delta t)^2 = frac\int_{-\infty}^{+\infty}(t-t_c)^2|x(t)|^2dt\int_{-\infty}^{+\infty}|x(t)|^2dt$.

In order to facilitate the calculations, and as the duration 'rms' is independent of the date, we will set $t_0 = 0$. In this case, $t_c \simeq \tau\frac{a^2+a\ cos(2\pi f_0\tau)e^{-\frac{\tau^2}{2T^2}}}{1+a^2+2a\ cos(2\pi f_0\tau)e^{-\frac{\tau^2}{2T^2}}}$

$(\Delta t)^2 = \frac{1}{E}\int_{-\infty}^{+\infty}(t^2-2t\,t_c+t_c^2)[(g(t))^2+2ag(t)g(t-\tau)+a^2(g(t-\tau))^2]dt$

By expanding, we get :

$$\begin{aligned}E(\Delta t)^2 = &\int_{-\infty}^{+\infty}t^2(g(t))^2dt+2a\int_{-\infty}^{+\infty}t^2g(t)g(t-\tau)dt+a^2\int_{-\infty}^{+\infty}t^2(g(t-\tau))^2\\ &-2t_c\int_{-\infty}^{+\infty}t(g(t))^2dt-4at_c\int_{-\infty}^{+\infty}tg(t)g(t-\tau)dt-2a^2t_c\int_{-\infty}^{+\infty}t(g(t-\tau))^2\\ &+t_c^2\int_{-\infty}^{+\infty}(g(t))^2dt+2at_c^2\int_{-\infty}^{+\infty}g(t)g(t-\tau)dt+a^2t_c^2\int_{-\infty}^{+\infty}(g(t-\tau))^2\end{aligned}$$

By making changes of variables, we get:

$$\begin{aligned}E(\Delta t)^2 = &\int_{-\infty}^{+\infty}t^2(g(t))^2dt+2a\int_{-\infty}^{+\infty}t^2g(t)g(t-\tau)dt+a^2\int_{-\infty}^{+\infty}(t+\tau)^2(g(t))^2\\ &-2t_c\int_{-\infty}^{+\infty}t(g(t))^2dt-4at_c\int_{-\infty}^{+\infty}tg(t)g(t-\tau)dt-2a^2t_c\int_{-\infty}^{+\infty}(t+\tau)(g(t))^2\\ &+t_c^2\int_{-\infty}^{+\infty}(g(t))^2dt+2at_c^2\int_{-\infty}^{+\infty}g(t)g(t-\tau)dt+a^2t_c^2\int_{-\infty}^{+\infty}(g(t))^2\end{aligned}$$

by rearranging:

$$\begin{aligned}E(\Delta t)^2 = &[t_c^2+a^2t_c^2+a^2\tau^2-2a^2t_c\tau]\int_{-\infty}^{+\infty}(g(t))^2dt+[-2t_c+2a^2\tau-2a^2t_c]\int_{-\infty}^{+\infty}t(g(t))^2dt+[1+a^2]\int_{-\infty}^{+\infty}t^2(g(t))^2dt\\ &+[2at_c^2]\int_{-\infty}^{+\infty}g(t)g(t-\tau)dt+[-4at_c]\int_{-\infty}^{+\infty}tg(t)g(t-\tau)dt+[2a]\int_{-\infty}^{+\infty}t^2g(t)g(t-\tau)dt\end{aligned}$$

$$E(\Delta t)^2 = \frac{A^2}{2}\sqrt{\frac{\pi}{2}}T\quad[(1+a^2)t_c^2+a^2\tau^2-2a^2t_c\tau+(1+a^2)T^2/4+(2at_c^2-2at_c\tau+a\tau^2/2+aT^2/2)cos(2\pi f_0\tau)e^{-\frac{\tau^2}{2T^2}}]$$

$$(\Delta t)^2 = \frac{t_c^2+(1+a^2)\frac{T^2}{4}+a^2((t_c-\tau)^2)\ +(2t_c^2-2t_c\tau+\tau^2/2+T^2/2)a\ cos(2\pi f_0\tau)e^{-\frac{\tau^2}{2T^2}}}{(1+a^2)+2a\ cos(2\pi f_0\tau)e^{-\frac{\tau^2}{2T^2}}}$$

$$(\Delta t)^2 = \frac{t_c^2+\frac{T^2}{4}+a^2((t_c-\tau)^2)\ +(2t_c^2-2t_c\tau+\tau^2/2)a\ cos(2\pi f_0\tau)e^{-\frac{\tau^2}{2T^2}}}{(1+a^2)+2a\ cos(2\pi f_0\tau)e^{-\frac{\tau^2}{2T^2}}}$$

Remark : When a becomes close to zero (very weak replica), we indeed find $(\Delta t)^2 \simeq \frac{T^2}{4}$.

Reminder : The following formulas have already been demonstrated above (and simplified in the case $t_0 = 0$) :

$$\int_{-\infty}^{+\infty}(g(t))^2dt \simeq \frac{A^2}{2}\sqrt{\frac{\pi}{2}}T$$

$$\int_{-\infty}^{+\infty}t(g(t))^2dt \simeq \frac{A^2}{2}\sqrt{\frac{\pi}{2}}Tt_0 \simeq 0$$

$$\int_{-\infty}^{+\infty}t^2(g(t))^2dt \simeq \frac{A^2}{2}\sqrt{\frac{\pi}{2}}T[(t_0)^2+T^2/4] \simeq \frac{A^2}{2}\sqrt{\frac{\pi}{2}}T\ \frac{T^2}{4}$$

$$\int_{-\infty}^{+\infty}g(t)g(t-\tau)dt \simeq \frac{A^2}{2}\sqrt{\frac{\pi}{2}}Tcos(2\pi f_0\tau)e^{-\frac{\tau^2}{2T^2}}$$

$$\int_{-\infty}^{+\infty}tg(t)g(t-\tau)dt \simeq \frac{A^2}{2}\sqrt{\frac{\pi}{2}}Tcos(2\pi f_0\tau)e^{-\frac{\tau^2}{2T^2}}(t_0+\tau/2) \simeq \frac{A^2}{2}\sqrt{\frac{\pi}{2}}Tcos(2\pi f_0\tau)e^{-\frac{\tau^2}{2T^2}}\tau/2$$

$$\int_{-\infty}^{+\infty}t^2g(t)g(t-\tau)dt \simeq \frac{A^2}{2}\sqrt{\frac{\pi}{2}}Tcos(2\pi f_0\tau)e^{-\frac{\tau^2}{2T^2}}(t_0^2+\tau^2/4+T^2/4) \simeq \frac{A^2}{2}\sqrt{\frac{\pi}{2}}Tcos(2\pi f_0\tau)e^{-\frac{\tau^2}{2T^2}}(\tau^2/4+T^2/4)$$

Peak frequency The peak frequency is the frequency for which the modulus of the Fourier transform is maximal. In the case of a complex Gabor wavelet, $|X(f)| \simeq AT\sqrt{\pi/2}\ e^{-\pi^2T^2(f-f_0)^2}\ |1+ae^{-2i\pi f\tau}|$

$|X(f)| \simeq AT\sqrt{\pi/2}\ e^{-\pi^2T^2(f-f_0)^2}\ \sqrt{1+a^2+2acos(2\pi f\tau)}$

This maximum will occur for the value of the frequency close to f_0 for which f is a multiple of $\frac{1}{\tau}$. If τ is large then the maximum will be very close to f_0. If τ is low The maximum can be relatively far from f_0, by an order of magnitude of 5 to 10% (see figure **??**).

Centroïde frequency The centroid frequency is calculated as the moment of order 1 of the frequencies, considering $|S(f)|^2$ as a density.

$f_c = \frac{\int_{-\infty}^{\infty} f|X(f)|^2df}{\int_{-\infty}^{\infty}|X(f)|^2df} = \frac{1}{E}\int_{-\infty}^{\infty} fA^2T^2\pi e^{-2\pi^2T^2(f-f_0)^2}(1+a^2+2acos(2\pi f\tau)df$

$Ef_c = A^2T^2\pi\int_{-\infty}^{\infty}(f+f_0)e^{-2\pi^2T^2f^2}(1+a^2+2acos(2\pi(f+f_0)\tau)df$

$Ef_c = A^2T^2\pi[(1+a^2)f_0\int_{-\infty}^{\infty}e^{-2\pi^2T^2f^2}+2a\int_{-\infty}^{\infty}(f+f_0)(cos(2\pi f\tau)cos(2\pi f_0\tau)-sin(2\pi f\tau)sin(2\pi f_0\tau)e^{-2\pi^2T^2f^2}df]$

$Ef_c = A^2T\sqrt{\frac{\pi}{2}}(1+a^2)f_0+2A^2T^2\pi af_0\ cos(2\pi f_0\tau)\int_{-\infty}^{\infty}cos(2\pi f\tau)e^{-2\pi^2T^2f^2}df-2A^2T^2\pi a\ sin(2\pi f_0\tau)\int_{-\infty}^{\infty}fsin(2\pi f\tau)e^{-2\pi^2T^2f^2}df]$

$Ef_c = A^2T\sqrt{\frac{\pi}{2}}[(1+a^2)f_0+2af_0\ cos(2\pi f_0\tau)e^{-\frac{\tau^2}{2T^2}}-\frac{a\tau}{\pi T^2}\ sin(2\pi f_0\tau)e^{-\frac{\tau^2}{2T^2}}]$

$f_c = f_0 - \frac{\frac{a\tau}{\pi T^2}e^{-\tau^2/2T^2}\sin(2\pi\tau f_0)}{1+a^2+2a\ e^{-\tau^2/2T^2}\cos(2\pi\tau f_0)}$

Bandwidth at -3 dB and -10 dB and quality factor at -3 dB The bandwidth at -3 dB, denoted $\Delta f_{-3\ dB}$, is calculated as the length of the frequency range during which the envelope of $X(f)$ is greater than the maximum value of X minus -3 dB, which is an approximation of the fact that This translates to $\frac{envelope\ of(f)}{maximum\ of\ X(f)} > \frac{1}{\sqrt{2}}$. As for the durations, the calculation of these values is complicated, essentially due to the oscillation of the spectrum of period $\frac{1}{\tau}$ and we pr éfŵill calculate the 'rms' bandwidth.

Bandwidth 'rms' The rms bandwidth is the second moment associated with the frequency distribution and is equal to $\Delta f = \sqrt{\frac{\int_{-\infty}^{+\infty}(f-f_c)^2|X(f)|^2df}{\int_{-\infty}^{+\infty}|X(f)|^2df}}$

Then $E(\Delta f)^2 = A^2T^2\pi\int_{-\infty}^{+\infty}(f-f_c)^2e^{-2\pi^2T^2(f-f_0)^2}(1+a^2+2acos(2\pi f\tau)df$

$E(\Delta f)^2 = A^2T^2\pi\int_{-\infty}^{+\infty}(f+f_0-f_c)^2e^{-2\pi^2T^2f^2}(1+a^2+2acos(2\pi(f+f_0)\tau)df$

$E(\Delta f)^2 = A^2T^2\pi\int_{-\infty}^{+\infty}(f^2+(f_0-f_c)^2+2f(f_0-f_c))e^{-2\pi^2T^2f^2}(1+a^2+2acos(2\pi f_0\tau)cos(2\pi f\tau)-2asin(2\pi f_0\tau)sin(2\pi f\tau))df$

$E(\Delta f)^2 = A^2T^2\pi[\int_{-\infty}^{+\infty}(f^2+(f_0-f_c)^2)e^{-2\pi^2T^2f^2}(1+a^2+2acos(2\pi f_0\tau)cos(2\pi f\tau))df-4asin(2\pi f_0)(f_0-f_c)\int_{-\infty}^{+\infty}fe^{-2\pi^2T^2f^2}sin(2\pi f\tau))df]$

$E(\Delta f)^2 = A^2T^2\pi[(f_0-f_c)^2(1+a^2)\frac{1}{\sqrt{2\pi}T}+(1+a^2)\int_{-\infty}^{+\infty}f^2e^{-2\pi^2T^2f^2}df+2a(f_0-f_c)^2\ cos(2\pi f_0\tau)\int_{-\infty}^{+\infty}e^{-2\pi^2T^2f^2}cos(2\pi f\tau)df$

$+2a\ cos(2\pi f_0\tau)\int_{-\infty}^{+\infty}f^2e^{-2\pi^{22}f^2}cos(2\pi f\tau)df-4asin(2\pi f_0\tau)(f_0-f_c)\frac{1}{\sqrt{2\pi}T}\frac{\tau}{2\pi T^2}e^{-\tau^2/2T^2}]$

$E(\Delta f)^2 = A^2T^2\pi[(f_0-f_c)^2(1+a^2)\frac{1}{\sqrt{2\pi}T}+(1+a^2)\frac{1}{\sqrt{2\pi}T}\frac{1}{4\pi^2T^2}+2a(f_0-f_c)^2\ cos(2\pi f_0)\frac{1}{\sqrt{2\pi}T}e^{-\tau^2/2T^2}$

$+2a\ cos(2\pi f_0)\frac{1}{\sqrt{2\pi}T}\frac{1}{4\pi^2T^2}e^{-\tau^2/2T^2}(1-\frac{2\tau^2}{\pi T^2})-4asin(2\pi f_0)(f_0-f_c)\frac{1}{\sqrt{2\pi}T}\frac{\tau}{2\pi T^2}e^{-\tau^2/2T^2}]$

$E(\Delta f)^2 = A^2T\sqrt{\frac{\pi}{2}}[(1+a^2+2acos(2\pi f_0\tau)e^{-\tau^2/2T^2})((f_0-f_c)^2+\frac{1}{4\pi^2T^2})-a\ cos(2\pi f_0)\frac{\tau^2}{\pi^3T^4}e^{-\tau^2/2T^2}-4asin(2\pi f_0)(f_0-f_c)\frac{\tau}{2\pi T^2}e^{-\tau^2/2T^2}]$

$(\Delta f)^2 = (f_0-f_c)^2+\frac{1}{4\pi^2T^2}-\frac{a\tau}{\pi T}\frac{cos(2\pi f_0)\frac{\tau}{\pi^2T^3}+2sin(2\pi f_0)\frac{f_0-f_c}{T}}{1+a^2+2acos(2\pi f_0\tau)}$

Quality factor 'rms' The 'rms' quality factor is $Q_{rms} = \frac{f_c}{\Delta f} =$ and can therefore be calculated explicitly using the above formulas.

Uncertainty product The uncertainty product or duration-bandwidth product 'rms' equals $P_{incert} = \Delta t \times \Delta f$ and can therefore be calculated explicitly.

Autocorrelation function The autocorrelation function is defined by $CS(r) = \int_{-\infty}^{+\infty}s(t)s^*(t+r)dt$ And so, for a real Gabor wavelet with replica, $C_x(r) = \int_{-\infty}^{+\infty}[g(t)+ag(t-\tau)][g^*(t+r)+ag^*(t+r-\tau)]dt$

$C_x(r) = \int_{-\infty}^{+\infty}g(t)g^*(t+r)dt+a\int_{-\infty}^{+\infty}g(t)g^*(t+r-\tau)dt+a\int_{-\infty}^{+\infty}g(t-\tau)g^*(t+r)dt+a^2\int_{-\infty}^{+\infty}g(t-\tau)g^*(t+r-\tau)dt$

$C_x(r) = C_g(r)+aC_g(r-\tau)+a\int_{-\infty}^{+\infty}g(u)g^*(u+\tau+r)du+a^2\int_{-\infty}^{+\infty}g(u)g^*(u+r)du$

$C_x(r) = (1+a^2)C_g(r)+aC_g(r-\tau)+aC_g(r+\tau)$

The figures and calculations of this report have been made in OCTAVE (Eaton et al. 2009).

References

Au, W. (1993). *The sonar of dolphin*. Springer.

de Bruin, M. and Kamminga, C. (2001). Uncertainty product of composite signals. *J. Phys. A: Math. Gen.*, (34):231–238.

Dubrovsky, N., Gladilin, A., Mohl, B., and Wahlberg, M. (2004). Modeling of the dolphinâs clicking sound source : The influence of the critical parameters. *Acoustical Physics*, 50(4).

Eaton, J., Bateman, D., and Hauberg, S. (2009). *GNU Octave version 3.0.1 manual: a high-level interactive language for numerical computations*. CreateSpace Independent Publishing Platform. ISBN 1441413006.

Gabor, D. (1946). Theory of communication. *Journal of the Institution of Electrical Engineers*, 93:429–441.

Goold, J. C. and Jones, S. E. (1995). Time and frequency domain characteristics whale of sperm clicks. *Journal of Acoustic society of America*.

Götz, T., Antunes, R., and Heinrich, S. (2010). Echolocation clicks of free-ranging chilean dolphins (cephalorhynchus eutropia). *The Journal of the Acoustical Society of America*, 128:563–6.

Kamminga, C., Cohen-Stuart, A., and Silber, G. (1996). Investigations on cetacean sonar xi : Intrinsic comparison of the wave shapes of some members of the phocoenidae family. *Aquatic mammals*, 22(1):45–55.

Kamminga, C., Kataoka, T., and Engelsma, F. (1986). Investigations on cetacean sonar vii : Underwater sounds of neophocaena phocaenoides of the japanese coastal population. *Aquatic mammals*, 12(2):52–60.

Kamminga, C., VanHove, M., Engelsma, F., and Terry, R. (1993). Investigations on cetacean sonar x : a comparative analysis of underwater echolocation clicks of inia spp. and sotalia spp. *Aquatic mammals*, 19(1):31–43.

Kyhn, L., Jensen, F., Beedholm, K., Tougaard, J., Hansen, M., and Madsen, P. (2010). Echolocation in sympatric peale's dolphins (lagenorhynchus australis) and commerson's dolphins (cephalorhynchus commersonii) producing narrow-band high-frequency clicks. *The Journal of experimental biology*, 213:1940–9.

Lammers, M. and Castellote, M. (2009). The beluga whale produces two pulses to form its sonar signal. *Bio. Lett.*, 5:297–301.

Malige, F., Patris, J., Buchan, S., Stafford, K., Shabangu, F., Findlay, K., Hucke-Gaete, R., Neira, S., Clark, C., and Glotin, H. (2020). Inter-annual decrease in pulse rate and peak frequency of southeast pacific blue whale song types. *Scientific reports*, 10:8121.

Mellinger, D. and Clark, C. W. (1997). Methods for automatic detection of mysticete sounds. *Marine and Freshwater Behaviour and Physiology*, 29: 1-4:163–181.

Patris, J., Malige, F., Glotin, H., Asch, M., and Buchan, S. (2019). A standardized method of classifying pulsed sounds and its application to pulse rate measurement of blue whale southeast pacific song units. *JASA, 146(4), October*.

Patris, J., Malige, F., Hamame, M., Glotin, H., Barchasz, V., Gies, V., Marzetti, S., and Buchan, S. (2023). Medium-term acoustic monitoring of patagonian coastal dolphins. *accepted by PeerJ*.

Reyes Reyes, M., Iniguez, M., Hevia, M., Hildebrand, J., and Melcon, M. (2015). Description and clustering of echolocation signals of commerson's dolphins (cephalorhynchus commersonii) in bahia san julian, argentina. *The Journal of the Acoustical Society of America*, 138:2046.

Reyes Reyes, V., Marino, A., Dellabianca, N., Hevia, M., Torres, M., Raya Rey, A., and Melcón, M. (2018). Clicks of wild burmeister's porpoises (phocoena spinipinnis) in tierra del fuego, argentina: Notes. *Marine Mammal Science*, 34.

Rihaczek, A. (1996). *Principles of High-Resolution Radar*. Artech House.

Rojas-Mena, R. (2009). *Caracterización del repertorio acústico del delfin chileno cephalorhynchus eutropia (gray,1846) y del delfin austral lagenorhynchus australis (peale, 1848) en la isla de chiloe, region de los lagos, chile.* Tesis de grado, Universidad Austral de Chile.

Tregenza, N. (2014). Cpod.exe: a guide for users. Technical report, Chelonia Ltd.

Ville, J. (1948). Théorie et application de la notion de signal analytique. *Cables et transmissions*, 1:61–74.

Wei, C., Au, W., and Ketten, D. (2020). Modeling of the near to far acoustic fields of an echolocating bottlenose dolphin and harbor porpoise. *J. Acoust. Soc. Am.*, 3:1790–1801.

Wiersma, H. (1982). Investigation on cetacean sonar iv : A comparison of wave shapes of odontocetes sonar signals. *Aquatic mammals*, 9(2).